IDŐJÁRÁS

QUARTERLY JOURNAL
OF THE HUNGARIAN METEOROLOGICAL SERVICE

CONTENTS

****

http://www.met.hu/Journal-Idojaras.php

VOL. 112 * NO. 2 * APRIL – JUNE 2008

IDŐJÁRÁS

Quarterly Journal of the Hungarian Meteorological Service

Editorial Office: Gilice tér 39, H-1182 Budapest, Hungary
P.O. Box 39, H-1675 Budapest, Hungary
E-mail: bozo.l@met.hu or antal.e@met.hu
Fax: (36-1) 346-4809

Indexed and abstracted in Science Citation Index Expanded™ and Journal Citation Reports/Science Edition
Covered in the abstract and citation database SCOPUS®

Subscription by

mail: IDŐJÁRÁS, P.O. Box 39, H-1675 Budapest, Hungary;
E-mail: kenderesy.k@met.hu or antal.e@met.hu

IDŐJÁRÁS

Quarterly Journal of the Hungarian Meteorological Service
Vol. 112, No. 2, April–June 2008, pp. 63–82

Hygroscopic behavior of Central European atmospheric background aerosol particles in summer

Kornelia Imre[1] and **Agnes Molnár**[2*]

[1]*Department of Earth and Environmental Sciences, University of Pannonia, P.O. Box 158, H-8201 Veszprém, Hungary; E-mail: kornelia@almos.uni-pannon.hu*

[2]*Air Chemistry Group, Hungarian Academy of Sciences, P.O. Box 158, H-8201 Veszprém, Hungary; E-mail: amolnar@almos.uni-pannon.hu*

(Manuscript received in final form March 7, 2008)

Abstract—The hygroscopic properties of size selected regional background aerosol were studied in 8 size ranges, from 62.5 nm to 16 μm. The mass of the aerosol samples was measured gravimetrically under controlled relative humidity (*RH*). The data showed important variation of the mass growth (*GM*) as a function of the size. In the fine mode, the highest growth was found at 86% *RH* in the smallest particle size range ($GM = 2.2$), while the lowest was found in the 0.25–0.50 μm size interval ($GM = 1.4$). In the coarse mode, the highest growth was found in the 1–4 μm ($GM = 2.1$) range. Based on the inorganic ion content of the samples, the water uptake of model aerosol (determined by the Aerosol Inorganics Model (AIM)) was also calculated; and the measured and calculated mass growth rates were compared. We found that fine range particles absorb less water than the modeled aerosol. In the coarse mode, the measured mass growth rate was often higher than the value calculated. Our results showed that in the fine mode the water deficiency (difference between measured and calculated water concentrations) is the function of the total carbon concentration (*TC*) of the samples (e.g., at 86% *RH*, 1 μg m^{-3} *TC* surplus results in a 2.86 μg m^{-3} decrease of water concentration). On the basis of mass growth factors, particle diameter growth rates (*G*) were derived. At K-puszta, *G* varied between 1.10 and 1.50 at 86% *RH*. Finally, the power-law function was fitted to both the measured (γ_m) and calculated (γ_c) data. With the application of multi-linear regression, we found that the fine mode γ_m can be estimated by the γ_c and the *TC* concentration, conversely to the coarse mode.

Key-words: aerosol particles, water uptake, organic and inorganic composition, size distribution

*Corresponding author

1. Introduction

The physical and chemical nature of aerosol particles is crucial to the control of the radiation budget of the Earth through direct scattering and absorption of the incoming solar radiation. Aerosol particles affect the structure and radiative properties of clouds by determining the number of cloud condensation nuclei. Besides the wavelength, the magnitude of scattered and absorbed radiation is the function of the particle size and chemical composition. Due to water-soluble components, the size of the particles is affected significantly by the ambient relative humidity. Their hygroscopic behavior is determined by the inorganic, as well as organic, species. Although the organic fraction of the particles is rather high, our knowledge on their effects on aerosol hygroscopicity is still limited (*Sjogren et al.*, 2007). Organic compounds can alter the hygroscopic growth by influencing the number of soluble ions available (Raoult's law) and by lowering the surface tension (Kelvin effect) (e.g., *Mircea et al.*, 2002, 2005).

Hygroscopic particle growth has been widely studied for 50 years. It was first measured by *Junge* at the beginning of 1950 (*Warneck*, 1999). *Winkler* and *Junge* (1972) and *Hänel* (1976) applied gravimetric method, while *Mészáros* (1971) studied the hygroscopic behavior of continental aerosol particles by means of optical microscopy. The results of these early studies already showed that hygroscopic growth of aerosol particles was smaller than that of pure salts. Also, the growth curves for continental aerosols were smoother than those of pure salts. Recently, hygroscopic and non-hygroscopic fractions of atmospheric aerosol were generally studied by Tandem Differential Mobility Analyzer (TDMA) systems (e.g., *McMurry* and *Stolzenburg,* 1989; *Svenningsson et al.,* 1994; *Swietlicki et al.,* 2000; *Ferron et al.*, 2005).

In numerous works, the hygroscopic properties of the individual inorganic salts (*Lee* and *Hsu*, 1998, 2000; *Gysel et al.*, 2002), organic compounds, and mixtures of the organic and inorganic particles (*Hämeri et al.*, 1998; *Chan et al.*, 1997; *Hansson et al.*, 1998; *Virkkula et al.*, 1999; *Sjogren et al.*, 2007) were studied. *Cruz* and *Pandis* (1997) concluded that pure dicarboxylic acids acted as CCN. *Mircea et al.* (2002, 2005) pointed out that the water-soluble fraction of aerosol particles influenced the surface tension of the droplets (particles). In several papers the effect of the organic cover of the particles (e.g., *Andrews* and *Larson*, 1993; *Pósfai et al.*, 2004) was studied.

Regarding the role of the organic species in aerosol hygroscopicity, different results and opinions have been published. On one hand, some authors proposed that organic compounds could be considered inactive in particle water uptake (e.g., *Pitchford* and *McMurry*, 1994; *Busch et al.*, 2002). However, more studies reported on how organic species modify the aerosol hygroscopicity (e.g., *Saxena et al.*, 1995; *Dick et al.*, 2000; *Cruz* and *Pandis*, 2000; *Choi* and *Chan*, 2002). *Saxena et al.* (1995) found that hygroscopic properties were affected by the aerosol type and origin: at a non-urban location the organic fraction

enhanced, while at an urban location organic matter reduced the water uptake of inorganic atmospheric aerosol. *Zhou et al.* (2001) proposed that more hygroscopic particles are most likely representative of the aged continental aerosol, while nearly hydrophobic particles originate from nearby combustion sources.

The aim of this work is to contribute to the understanding of the hygroscopic properties of atmospheric aerosol. In this study three problems are considered:

- Determination of hygroscopic growth of ambient aerosol particles with respect to their size distribution.
- Estimation of the effect of organic compounds on hygroscopicity.
- Modeling the hygroscopic growth of the particles as the function of their size and chemical composition.

2. Experimental

In the summer of 2001 and 2002, 13 size-selected ambient aerosol samples were taken at K-puszta station ($\varphi = 46.99°$, $\lambda = 19.55°$, 125 m a.s.l.), Hungary. The sampling site belongs to the GAW and EMEP monitoring networks. It is located on a forest clearing on the Great Hungarian Plain about 70 km south-east from Budapest. The closest town (Kecskemét) is 15 km SE of the station. Since this site is relatively far from direct anthropogenic sources, K-puszta is considered to be a regional background air pollution monitoring station. The representativeness of aerosol measurements at this station is discussed in detail by *Geresdi et al.* (2006).

The air was sampled by a 9-stage Berner impactor (*Berner*, 1984) at a height of 10 m, in order to avoid the direct impact of the surrounding sandy soil. The lower cut-off diameters of the impactor stages are 0.0625, 0.125, 0.25, 0.5, 1, 2, 4, 8, 16 μm at a sampling rate of 31.3 l min^{-1}. The aerosol particles were captured on Al-foils. In the summer of 2001, five samples (from July 27 to August 16) were collected. In 2002 (from June 28 to July 24) the number of samples was eight (sampling details are in *Table 1*). For the sake of reliable mass measurements, the duration of the sampling varied between 3–7 days.

In our experiments, the gravimetric method was applied for the determination of the mass change of aerosol particles due to their water uptake. Mass measurements were carried out by means of a Sartorius microbalance (detection limit is 10 μg), which was placed into an isolated chamber. The relative humidity of the chamber was controlled by saturated solutions of different salts ($Mg(NO_3)_2 \cdot 6\ H_2O$ (51%); NH_4NO_3 (64%); NaCl (76%); NH_4Cl (80%); KCl (86%)), as well as silica gel. The relative humidity was precisely measured by a hygrograph, which was calibrated in a climate chamber at the Hungarian Meteorological Service.

To validate this gravimetric method, the water uptake of ammonium sulfate measured gravimetrically, as well as determined on the basis of thermodynamic approach (using the Aerosol Inorganics Model (AIM) (*Clegg et al.*, 1998)) is summarized. The vaporized solution of ammonium sulfate was dried at $RH < 30\%$, then the dry mass (2.06 mmol) and the mass change (water uptake) were measured at the above mentioned *RH*s. As it is well known, the deliquescence relative humidity of ammonium sulfate is around 80% *RH*. Below this *RH*, both the calculated and measured water mass were zero. At 80, 86, and 90% *RH*s, the calculated water-uptake was 7.9, 10.7, and 14.4 mmol, respectively, while in the case of gravimetric analysis the corresponding values were 7.9, 10.5, and 14.5 mmol, respectively. We concluded that the data from gravimetric analysis are in good agreement with calculated values.

Table 1. Sampling details

Sample number	Sampling date	Air volume (m^3)
S1	July 27–July 31, 2001	163.5
S2	Aug 04–Aug 07, 2001	152.3
S3	Aug 08–Aug 10, 2001	112.4
S4	Aug 11–Aug 13, 2001	113.0
S5	Aug 14–Aug 16, 2001	112.2
S6	June 28–July 04 *d*, 2002	172.4
S7	June 28–July 05 *n*, 2002	122.8
S8	July 05–July 11 *d*, 2002	183.6
S9	July 05–July 12 *n*, 2002	106.4
S10	July 12–July 18 *d*, 2002	187.9
S11	July 12–July 19 *n*, 2002	113.2
S12	July 19–July 24 *d*, 2002	162.6
S13	July 19–July 24 *n*, 2002	79.4

Note: *d* and *n* denote daytime and nighttime sampling, respectively

In this study the following protocol was applied.

Before sampling: The mass of unloaded Al-foils was measured under low relative humidity (30%). The impactor substrates were generally kept in the chamber for more than 48 hours in order to reach thermodynamic equilibrium. After weighting, the Al-foils were packed and stored separately until sampling.

Sampling: The pre-weighted Al-foils were placed into the Berner impactor. After sampling, the Al-foils were carefully packed separately and were stored frozen until further processing and analysis.

After sampling: The dry mass, as well as the mass change of size-selected aerosol (as the function of relative humidity) were measured. The samples were kept at a given relative humidity for more than 48 hours in

order to reach equilibrium with their surroundings. The total aerosol mass collected on the impactor substrates was in the range of 50–780 μg. The standard deviation of parallel mass measurements was generally below 10%, as shown in *Table 2*.

Table 2. Dry mass (average ± standard deviation) of aerosol samples

Sample number	Particle mean diameter (μm)							
	0.088	**0.18**	**0.35**	**0.71**	**1.4**	**2.8**	**5.7**	**11.3**
S1	53±7	230±14	730±42	683±15	150±3	227±15	157±7	130±3
S2	100±11	273±12	640±30	473±6	75±7	197±6	278±12	83±6
S3	210±21	370±17	690±30	427±15	103±7	307±14	370±26	323±7
S4	240±5	305±7	520±28	505±7	390±8	195±7	210±4	70±7
S5	160±3	293±12	780±16	613±21	197±7	280±6	307±15	273±6
S6	103±15	363±10	647±6	467±6	137±6	367±6	363±6	313±6
S7	80±12	195±6	493±21	413±15	170±6	333±6	270±15	333±15
S8	40±20	227±6	547±12	740±10	123±6	230±12	223±12	220±6
S9	58±6	137±12	587±12	573±6	183±6	193±10	233±6	133±6
S10	77±21	223±10	807±10	750±6	187±12	307±10	327±6	290±20
S11	27±6	97±20	447±23	573±12	183±6	227±6	217±21	153±6
S12	75±12	183±6	557±25	547±11	180±17	127±87	177±12	125±6
S13	29±6	51±6	260±6	287±12	170±6	107±6	150±10	90±6

Finally: The chemical composition of the impactor samples was determined. Al-foils were cut into four parts. One part was used for total carbon analysis; the second part was extracted in water to dissolve water-soluble inorganic ions. (The rest of the samples were reserved for further analysis.) The extraction of the samples was performed in 2 ml high purity (MilliQ) water. Then the extracts were filtered through a membrane filter (Millipore, 0.22 μm) in order to remove non-dissolved particles suspended in the solution. The concentrations of inorganic ions (ammonium, potassium, sodium, calcium, magnesium, chloride, sulfate, and nitrate) were determined by capillary electrophoresis and ion chromatography. The detection limits of the inorganic ion concentrations (at a signal-to-noise ratio of 3) were <100 μg l^{-1} for both capillary electrophoresis (details in *Temesi et al.,* 2001) and ion chromatography. The TC concentration of the aerosol samples was measured as carbon dioxide by the catalytic combustion method in oxygen at 680 °C, using the Astro Model 2100 TOC solid-analyzer. The calibration solution was potassium hydrogen phthalate and the detection limit of carbon measurement was 2 μgC (at a signal-to-noise ratio of 3).

3. *Results and discussion*

3.1. Dry mass size distribution and chemical composition

In *Fig. 1*, the size and chemical distribution of dry aerosol particles is presented. During the sampling period the average total dry mass concentration was 17.4 μg m^{-3}, with a standard deviation of 4.5 μg m^{-3} (marked as std. in the following text). The aerosol mass size distribution was generally bimodal. The majority of the dry mass a ccumulated in the fine size range with 62% (std. 6%) of the total mass found in PM_1. This high fraction indicates the importance of aged aerosol over this site. In several cases (see *Fig. 1*), a relatively high aerosol mass was measured in particles with diameter smaller than 0.1 μm, which is probably due to new particle production.

In *Fig. 1* the concentrations of the main chemical components (sulfate, nitrate, ammonium, and total carbon (*TC*)) are also shown. The total mean sulfate concentration was 2.9 μg m^{-3} (std. 1.2 μg m^{-3}), almost 90% of this component accumulated in PM_1, mostly in the range of 0.25–1.0 μm. The size distribution of ammonium was similar to sulfate, while nitrate was detected mainly in the coarse mode. Other ions (chloride, sodium, calcium, potassium, and magnesium) were also analyzed in the samples, and the sum of their concentration is shown in *Fig. 1* under "other ions". Average total carbon concentration amounted to 4.4 μg m^{-3} (std. 1.5 μg m^{-3}), around 60% of which was measured in the fine fraction, with the highest concentration in the range of 0.25–0.50 μm. It should be mentioned that carbonaceous compounds generally dominate the chemical composition of $PM_{0.1}$.

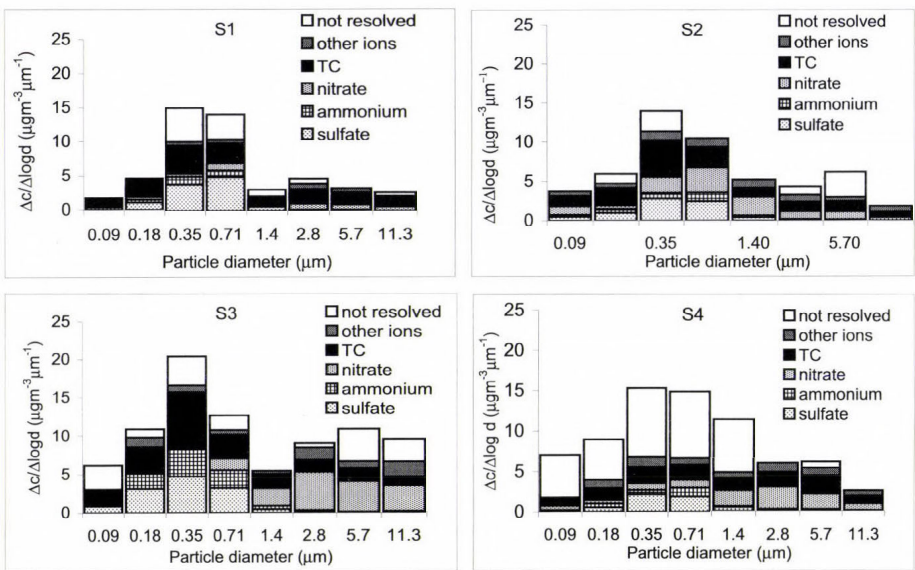

→

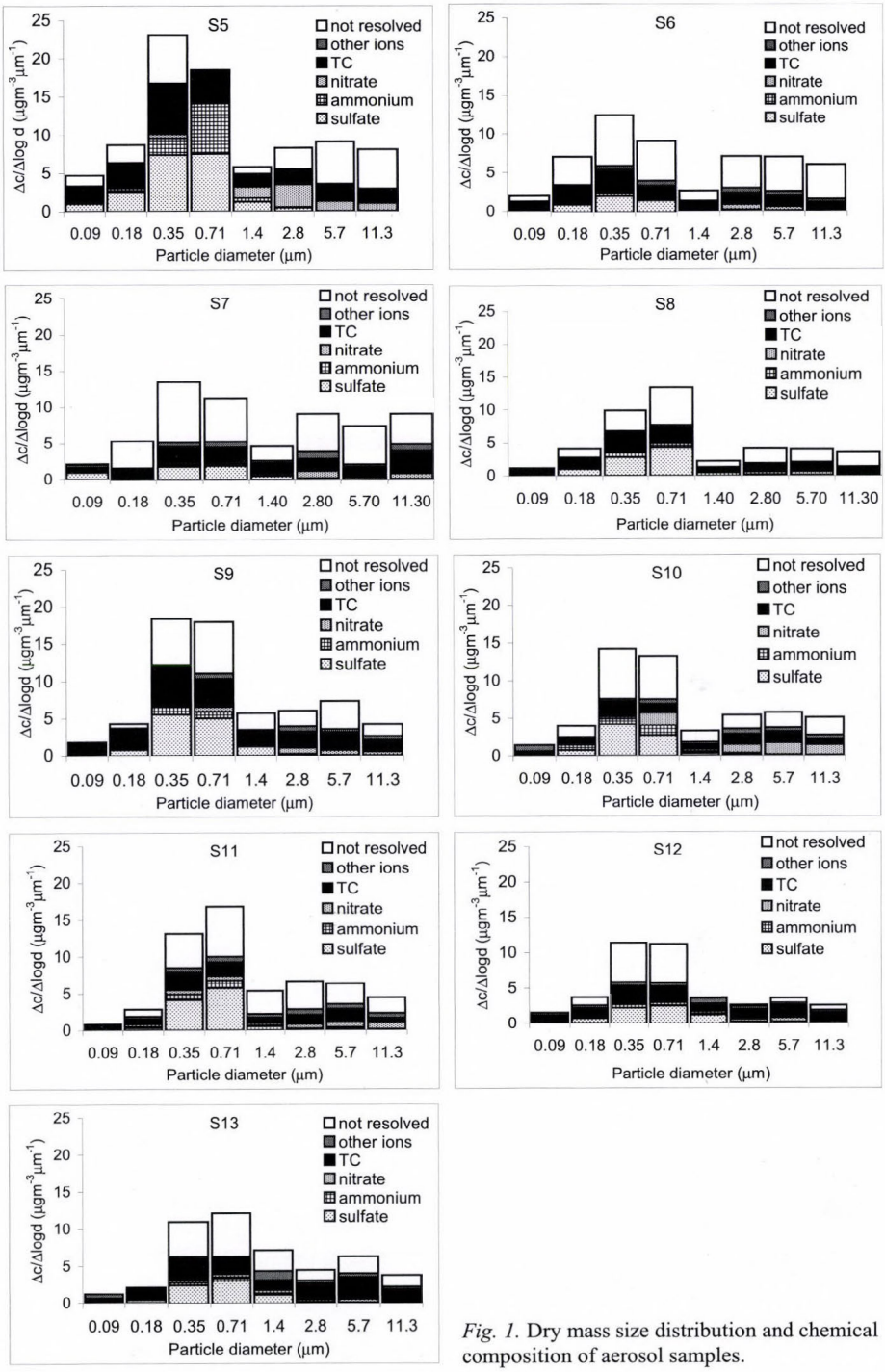

Fig. 1. Dry mass size distribution and chemical composition of aerosol samples.

3.2. *Measured and calculated mass growth*

Due to the hygroscopic behavior of atmospheric aerosol particles, the mass of the aerosol samples increased with increasing relative humidity. In *Fig. 2* the change in mass size distribution due to water absorption is presented for 4 selected samples. Generally, the mass change of the fine particles became significant above 80–86% *RH*, which is higher than the deliquescence *RH* of the most important inorganic salts. This is similar to results published earlier (e.g., *Winkler* and *Junge*, 1972; *Hänel*, 1976; *Hämeri et al.*, 1998; *Chan et al.*, 1997; *Hansson et al.*, 1998; *Virkkula et al.*, 1999; *Sjogren et al.*, 2007). The measured mass growth factors ($GM = M/M_{dry}$) at 86% relative humidity are presented in *Table 3* in the columns denoted by "m" (measured). The data (both in *Fig. 2* and *Table 3*) show important variations of the mass growth as a function of the size. Below 1 μm, the highest growth was found in the smallest particle size range (average: 2.2). Meanwhile, the lowest values were obtained in the 0.25–0.50 μm size interval (average 1.4). It should be noted that the low hygroscopic mass growth rate occurred with high total carbon concentration. In the coarse mode ($1 < d < 16$ μm), the highest growth was found in the range of 1–4 μm (average 2.1). More than 30 years ago *Mészáros* (1971) reported that hygroscopicity of the large and giant particles ($d > 0.4$ μm) decreased with increasing size. Our results differ from this data, probably due to the significant change in inorganic (mainly ammonium sulfate) salt concentrations over this time period (*Mészáros* and *Horváth*, 1984).

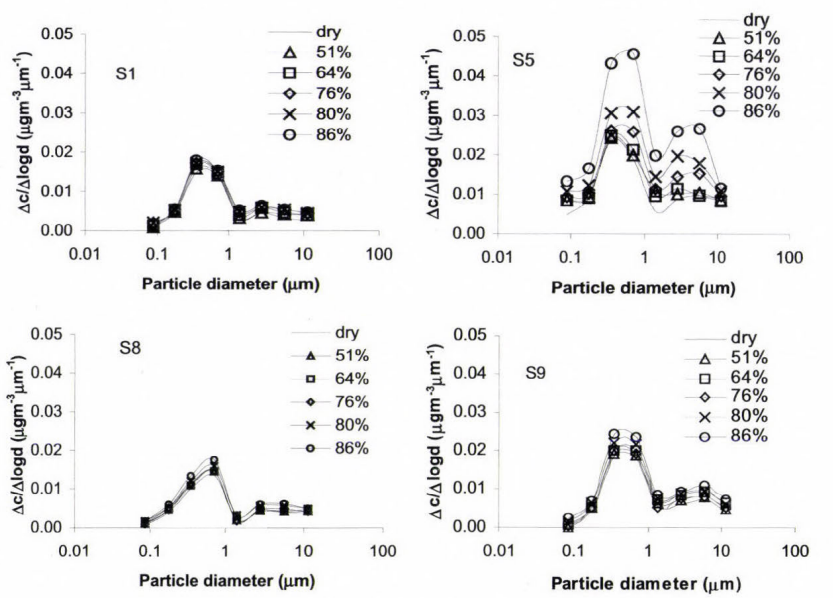

Fig. 2. Change in mass size distribution as the function of relative humidity.

On the basis of inorganic constituents, the mass growth of the particles in different size ranges was calculated by means of the AIM (*Clegg et al.,* 1998). This model gives the water uptake of a model aerosol (composed of inorganic ions: sulfate, nitrate, chloride, ammonium, potassium, sodium, calcium, and hydrogen) as the function of relative humidity. In the calculation we used the ion concentrations (except hydrogen) that were determined analytically in the size selected aerosol samples. The hydrogen concentration was calculated from the ion balance. We have to note that this model gives information on the Raoult-term, while the curvature effect of the particles is not involved. However, considering the aerosol size range evaluated in this work, this latter effect could only be important in the case of the first impactor stages (size range: 0.0625–0.125 μm) (*Maßling et al.*, 2003; *Ferron et al.*, 2005).

Table 3. Mass growth of particles at 86% *RH* (* denotes: data are not available)

Sample number	Particle mean diameter (μm)															
	0.088		0.18		0.35		0.71		1.4		2.8		5.7		11.3	
	m	c	m	c	m	c	m	c	m	c	m	c	m	c	m	c
S1	2.0	2.3	1.6	1.8	1.5	1.7	1.4	2.2	2.7	1.5	1.5	2.2	1.7	2.1	1.8	2.0
S2	1.9	3.6	1.2	1.7	1.3	2.1	1.9	2.7	5.4	7.1	5.3	5.5	*	*	5.2	5.9
S3	2.0	1.4	1.7	1.7	1.1	1.6	4.6	11.1	*	*	2.4	2.8	*	*	2.3	2.7
S4	1.1	1.6	1.1	1.5	1.2	1.7	1.5	1.7	1.7	2.0	1.4	4.5	1.5	2.9	1.4	3.8
S5	2.3	8.2	1.4	1.8	1.3	2.7	1.7	3.0	2.5	2.4	2.4	9.2	2.0	1.6	1.3	1.5
S6	1.1	1.3	1.1	1.4	1.1	1.4	1.1	1.4	1.2	1.3	1.2	1.1	1.1	1.1	1.0	1.0
S7	1.0	2.3	1.0	1.1	1.1	1.4	1.2	1.5	1.0	1.4	1.2	1.0	1.0	1.0	1.1	1.1
S8	2.4	2.5	1.5	2.0	1.3	2.1	1.3	2.3	1.4	2.0	1.5	1.2	1.5	1.1	1.4	1.1
S9	*	*	1.6	1.7	1.3	2.2	1.3	2.1	1.4	2.1	1.6	1.1	1.5	1.1	1.7	1.2
S10	5.9	3.2	2.2	*	2.0	3.0	*	2.4	2.8	1.7	3.2	1.4	2.4	1.1	1.7	1.1
S11	*	3.7	3.8	1.8	2.0	3.2	1.9	3.4	2.0	1.7	1.9	1.7	1.8	*	2.2	1.5
S12	2.4	3.4	1.2	2.3	1.1	2.4	1.2	2.6	1.5	3.4	2.5	1.4	1.4	1.4	1.6	1.3
S13	*	*	2.4	6.0	1.2	1.7	1.3	1.2	1.3	*	1.6	*	1.5	*	1.4	*
Average	**2.2**	**3.1**	**1.7**	**2.1**	**1.4**	**2.1**	**1.7**	**2.9**	**2.1**	**2.4**	**2.1**	**2.8**	**1.6**	**1.5**	**1.8**	**2.0**
σ	1.4	1.9	0.8	1.3	0.3	0.6	1.0	2.6	1.2	1.7	1.1	2.5	0.4	0.6	1.1	1.5

The "calculated" hygroscopic mass growth of the samples was estimated by the addition of measured aerosol dry mass and modeled water uptake (AIM calculations from the inorganic content of the samples) at different relative humidities. In *Table 3*, the calculated results of hygroscopic mass growth of model aerosol at 86% *RH* are presented in columns denoted by "c". The calculated mass growth rate shows a similar size distribution as the measured values (see the average mass growth data). However, in the fine size range the measured mass growth factors are generally lower (20–40%) than the calculated

ones. This indicates that the ambient aerosol is less hygroscopic than the model particles, probably due to their carbonaceous constituents. In the coarse mode, mainly above 2 μm, the mass growth measured is often higher than the value calculated. The ratio of measured and calculated mass growth varies within a rather broad range (26–232%). It is possible that other hygroscopic material besides inorganic salts can also be present in these particles that are not taken into account in the AIM model.

The role of carbonaceous compounds in the control of the hygroscopicity of the particles could be studied, if the difference between measured and calculated water concentration (water deficiency) is related to the total carbon concentration (*TC*) of the samples. In *Fig. 3* the water deficiency at different relative humidities, both for fine (d <1 μm) and coarse (d >1 μm) particles, is presented as the function of *TC* concentration. In the fine mode, a statistically significant relationship was found (probability level >95%) between the parameters. The data show that *TC* significantly affects the water-uptake of the particles. In other words, a higher *TC* concentration results in higher water deficiency. Moreover, besides *TC* concentration, the deficiency of water-uptake of the particles is also affected by the relative humidity. Our results indicate that the higher the relative humidity, the more significant the water deficiency. Regarding linear regression equations (see in *Fig. 3*) at 51%, 64%, 76%, 80%, and 86% *RH*, a 1 μg m^{-3} surplus in *TC* concentration results in a 0.75 μg m^{-3}, 1.20 μg m^{-3}, 1.67 μg m^{-3}, 2.08 μg m^{-3}, and 2.86 μg m^{-3} decrease in the absorbed water mass concentration, respectively. Finally, we have to note that no statistically significant relationship was found between *TC* and water deficiency in the coarse mode, as shown in *Fig. 3*.

The results of laboratory and field studies indicated that organic matter can influence the water uptake of the particles. In laboratory experiments, small carboxylic and multi-functional acids enhanced the water uptake of mixed particles (*Cruz* and *Pandis*, 2000; *Choi* and *Chan*, 2002; *Prenni et al.*, 2003). Field measurements also showed that organic species in aerosol particles can contribute to water absorption (*Dick et al.*, 2000; *Saxena et al.*, 1995). On the other hand, *Choi* and *Chan* (2002), *Cruz* and *Pandis* (2000), and *Saxena et al.*, (1995) reported that mainly in urban environments the organic fraction can reduce the water uptake of the inorganic compounds. Differences in the hygroscopic behavior between urban and non-urban particles are thought to be the result of aerosol ageing processes and the presence of polar organic species (*Alfarra et al.*, 2004; *Aklilu et al.*, 2006). Our results showed, however, that even in the regional background air, the carbonaceous content of the particles could significantly diminish the water absorption of the inorganic fraction.

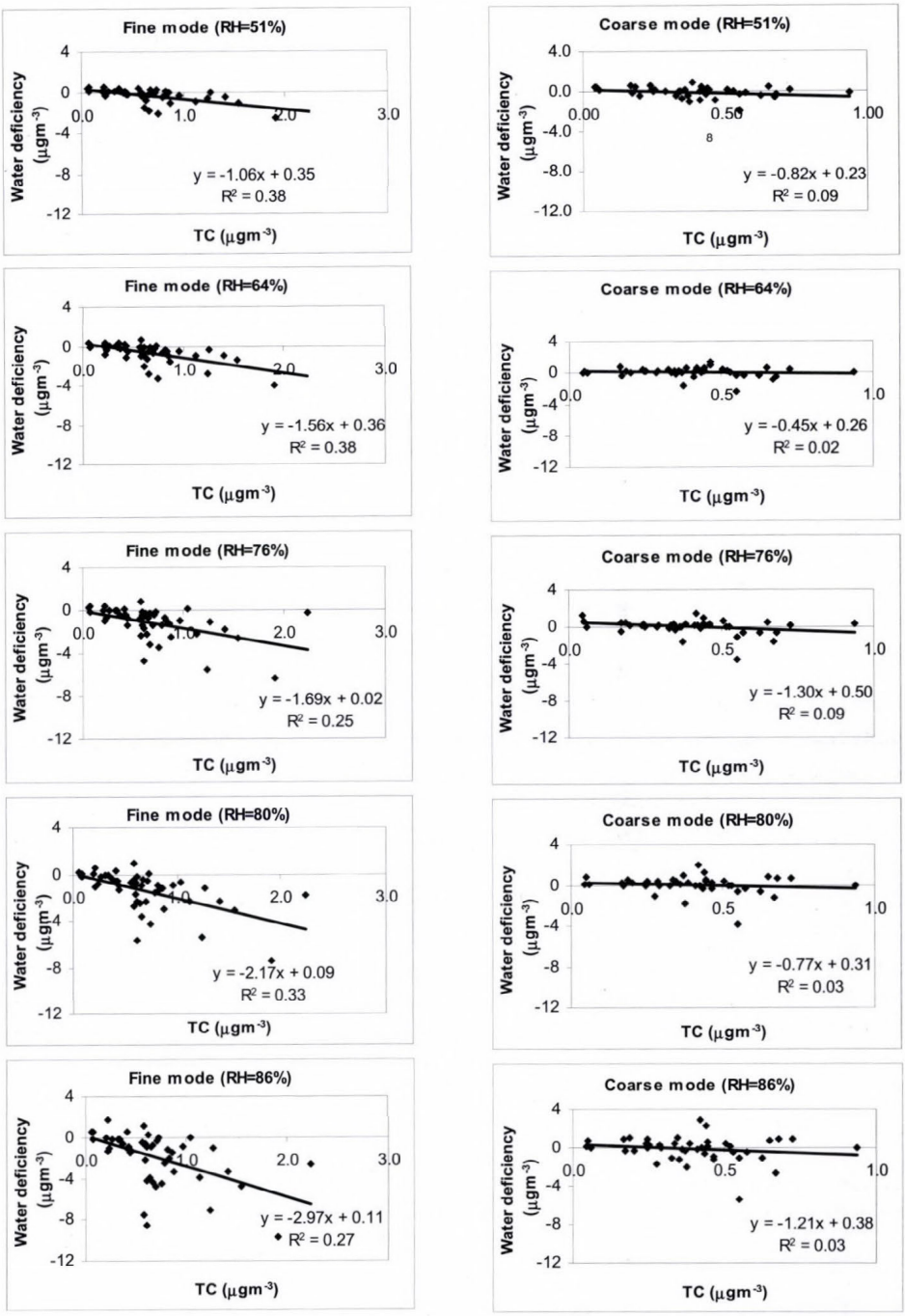

Fig. 3. Water deficiency as the function of total carbon concentration and relative humidity.

3.3. Growth in particle size

In order to compare our results to the hygroscopic growth factors published in the literature, the measured and calculated mass growth was converted into particle growth. Mass growth (GM) and particle size growth (G) factors are defined as:

$$GM_{RH} = \frac{M_{RH}}{M_{dry}} \quad \text{and} \quad G_{RH} = \frac{d_{RH}}{d_{dry}}, \tag{1}$$

where M and d denote the particle mass and particle diameter at a given RH compared to the dry values, respectively. In the calculation, the geometric mean aerodynamic diameter of each impactor stage was considered as the characteristic size of the particles. The conversion of mass growth to particle growth is possible if we consider that:

$$GM_{RH} = \frac{\rho_{RH}}{\rho_{dry}} \cdot \frac{d_{RH}^3}{d_{dry}^3} = \frac{\rho_{RH}}{\rho_{dry}} \cdot G_{RH}^3 . \tag{2}$$

Unfortunately, the estimation of the dry particle density (ρ_{dry}) as well as the particle density at a given relative humidity (ρ_{RH}) is rather uncertain. Concerning dry particle density, few data can be found and these data usually correspond to a certain particle size (e.g., *Stein et al.,* 1994). Stein and co-workers applied TDMA to determine the particle densities. They found that dry particle density for particles smaller than 0.236 μm is in the range of 1.74–1.78 g cm^{-3} within an uncertainty of 4%. In this work 1.76 g cm^{-3} dry particle density was used, which is close to the density of ammonium sulfate (e.g., *Sjogren et al.,* 2007).

To estimate the change in particle density due to water-uptake, further consideration is necessary. Although the absorbed water mass is directly measured, the consideration of the change in particle volume is not evident since the volumes of dry particle and water are not simply additive. However, several workers in the field generally assumed this additivity (e.g., *Hitzenberger et al.,* 1999; *Ferron et al.,* 2005). We also applied this assumption in further calculations:

$$\frac{\rho_{RH}}{\rho_{dry}} = \frac{M_{RH} \cdot \rho_{water}}{M_{dry} \cdot \rho_{water} + M_{water} \cdot \rho_{dry}} . \tag{3}$$

In *Fig. 4a* the size distributions of particle growth (G) are presented at 51%, 76%, and 86% RHs. According to these data, in the range of 0.125–0.500 μm, G

is characterized by a local minimum at all *RH*s. These particle growth factors can be compared to the data published by different authors. At low *RH* (50–55%) in marine air (*Maßling et al.*, 2003; *Zhou et al.*, 2001), the particle growth was more important than in the case of our samples. Data from AEROSOL99 – INDOEX (*Maßling et al.*, 2003) and Arctic Ocean Expedition (*Zhou et al.*, 2001) projects show increasing growth rates (G = 1.20–1.27 and 1.13–1.17, respectively) in the ranges of 50–250 nm and 50–165 nm, respectively. In approximately the same size range we obtained smaller growth rates (1.04–1.23), which decreased with the increasing particle size. At 70–76% *RH* we could draw similar conclusions as before: at K-puszta the aerosol particles were less hygroscopic ($G_{(76\%)}$ = 1.06–1.28) than the marine aerosol (AEROSOL99 – INDOEX (*Maßling et al.*, 2003), $G_{(75\%)}$ = 1.36–1.46 and 1.18–1.20 for more and less hygroscopic particles, respectively; also for the Arctic Ocean Expedition (*Zhou et al.*, 2001), $G_{(70\%)}$=1.23–1.29).

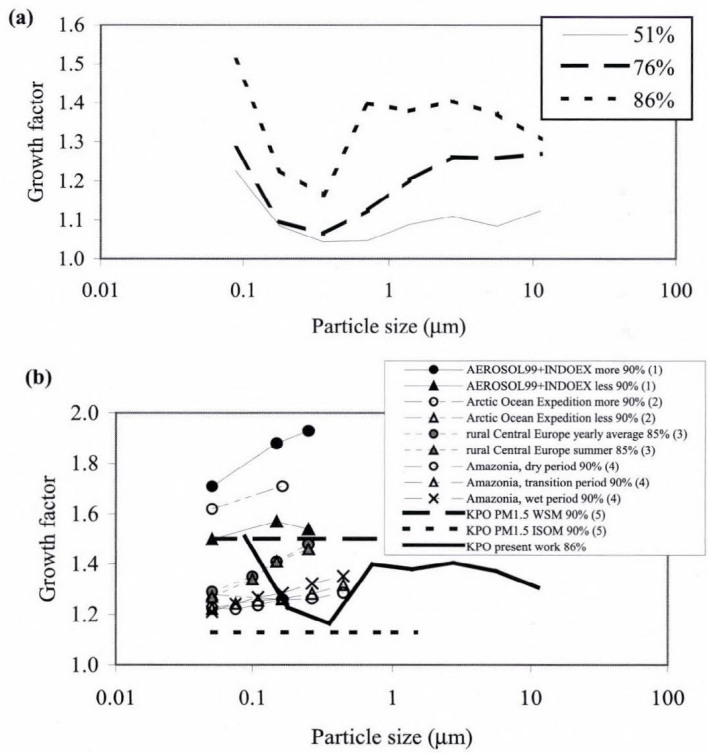

Fig. 4. Hygroscopic growth of aerosol particles as the function of the size. (a) At K-puszta, at 51%, 76%, and 86% *RH*. (b) Comparison of rural and background data at 86–90% *RH*. The referred publications are: (1) *Maßling et al.*, 2003; (2) *Zhou et al.*, 2001; (3) *Ferron et al.*, 2005; (4) *Rissler et al.*, 2006; (5) *Gysel et al.*, 2004.

In *Fig. 4b*, the size distribution of the growth factor at 85–90% relative humidity is presented. Along with our results, hygroscopic growth rates published by different authors are also plotted. These data also show that marine (oceanic) aerosol is more hygroscopic than the particles from the continental air. The growth factor of continental aerosol ranges between 1.13 and 1.50. These (lower and upper) limits correspond to the growth rate of ISOM (isolated water-soluble atmospheric humic matter, which is the less hydrophilic water soluble organic matter) and WSM (water soluble inorganic and organic matter) constituents of the aerosol sampled at K-puszta ($PM_{1.5}$; *Gysel et al.*, 2004). It is interesting to note that all growth rates referring to continental aerosol can be found in this range independently from the particle size and the sampling site. In studying our data we found that, between 125 and 500 nm, the hygroscopicity of the particles is rather similar to ISOM. This indirectly indicates that atmospheric humic matter may dominate in the chemical composition of these particles. On the other hand, in the smaller and larger fine particles (62.5–125 nm and 0.5–1.0 μm) water-soluble compounds (both inorganic and organic) are the most important constituents.

3.4. Modeling of size selected particle growth as a function of relative humidity

Consideration of the hygroscopic growth of aerosol particles in different processes (e.g., radiative forcing estimations) is very important. For the sake of simplicity and consistency, model functions describing the hygroscopic behavior of the aerosol particles are introduced. Particle growth G is generally and simply estimated as the function of relative humidity (RH in percentage). In this work we applied the following power-law function approach frequently proposed (e.g., *Zhou et al.*, 2001):

$$G(RH) = 10^{a} \cdot \left(\frac{1 - RH}{100}\right)^{-\gamma}. \tag{4}$$

In *Table 4* the summary of the fitted γ exponent and 10^{a} parameters are given for the measured, as well as calculated data sets. The growth rate is mostly governed by γ, since 10^{a} varies around 1. It can be seen that if γ is close to zero, the hygroscopicity of the particles is weak. The results in *Table 4* show that the measured particle growth (γexponent) strongly depends on the particle size. The obvious reason for this variation is the difference in chemical composition of the particles, which is indicated by the different γ values of aerosol particles with similar sizes. During the AEROSOL99 – INDOEX project (*Maßling et al.*, 2003), the mean value of the exponent was 0.230, 0.257, and 0.269 in the cases of 50 nm, 150 nm, and 250 nm sized particles, respectively. Meanwhile, *Zhou et al* (2001) published γ values of 0.201 ($d = 50$ nm) and 0.228 ($d = 165$ nm). *Gysel et al.* (2004) found that the mean γ exponent of ISOM and WSM in $PM_{1.5}$ was

0.064 and 0.196, respectively. The exponents obtained from our samples are within these latter two values, similarly to the particle growth rates (see above). Note that in the case of ammonium sulfate, the value of γ is 0.218 (*Sjogren et al.*, 2007).

Table 4. Parameters of power-law functions in different particle sizes for both measured and calculated data sets

Geometric particle diameter (μm)	Measured		Calculated	
	gamma	10^c	gamma	10^c
0.088	0.185	1.02	0.273	0.92
0.18	0.096	0.98	0.164	0.93
0.35	0.078	0.97	0.206	0.93
0.71	0.182	0.91	0.268	0.90
1.4	0.178	0.95	0.205	0.96
2.8	0.201	0.94	0.192	0.96
5.7	0.196	0.93	0.092	0.99
11.3	0.147	0.98	0.140	0.96

In *Fig. 5* the size dependence of "measured" particle growth – estimated by power-law fit – at 86% *RH* is presented. In the fine size range, particles in the smallest size interval (0.0625–0.125 μm) were found to be the most hygroscopic ($G_{(86\%)} \approx 1.5$). This size range was followed by the less hygroscopic particles in the 0.125–0.50 μm interval ($G_{(86\%)} = 1.10$–1.20), where γexponents were closest to zero (see also *Table 4*). The particles in the remaining size intervals showed similar hygroscopicity; their growth rate varied between 1.30 and 1.40. In *Table 4* the γ parameter is also given for the "calculated" data sets; and these data (at 86% RH) are plotted in *Fig. 5*.

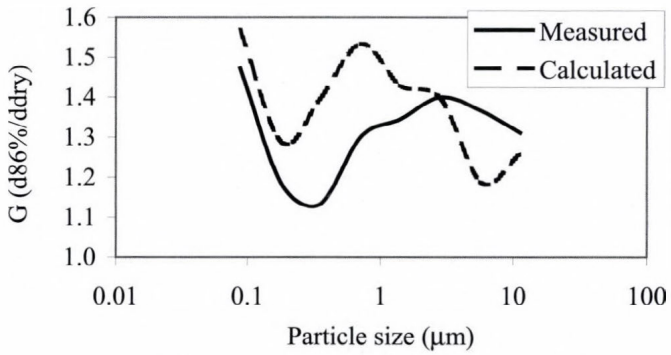

Fig. 5. Measured and calculated growth rate (86% *RH*) as the function of the size.

The size distribution of the "calculated" growth factor shows similarities to the "measured" values; however, in the fine size range the "calculated" growth factors are consistently higher than the "measured" ones. In the coarse mode, no similarities were found. Above 2.8 μm, the "measured" particle growth was underestimated by the growth rates "calculated". As it was mentioned before, it indicates that more compounds – other than those analyzed – can significantly contribute to the hygroscopic growth of the coarse particles. In the fine mode, the best agreement between "calculated" and "measured" data is found in stage 1 (smallest particles), while above this size the difference is rather high. It is supposed that this alteration can be attributed to the effect of carbonaceous compounds, which have the highest concentration in these size ranges (see *Fig. 1*).

One can suppose that the γ exponent is mainly controlled by the chemical composition of the particles. (Note: the curvature effect of the aerosol particles plays an important role only under 100 nm (*Maßling et al.*, 2003; *Ferron et al.*, 2005)). If we suppose that we have information on the concentration of all the important chemical compounds that are responsible for the control of hygroscopic growth, then we can assume that the measured γ exponent (γ_m in the following) can be estimated by the inorganic ion and total carbon concentrations of the aerosol particles. Further, we can presume that:

- The hygroscopic behavior of the inorganic compounds is well estimated by the AIM model. This means that the "calculated" γ exponent (denoted by γ_c in the following) correctly described the water uptake of inorganic ions.
- The hygroscopic effect of carbonaceous compounds can be estimated by the *TC* concentration.

If we accept the above assumptions, then γ_m could be estimated as the function of the γ_c and the *TC* concentration. As a first approximation, the linear function of two variables is considered:

$$\gamma_m = m_1 \cdot \gamma_c + m_2 \cdot TC + b. \tag{5}$$

The calculation is based on a multilinear approach, where m_1 and m_2 are coefficients, parameter b could be considered as the hygroscopic effect of other constituents that are not determined. The statistical significance (at the probability level of 99%) is checked by F-distribution. The results show a statistically significant relationship among the parameters considered, both for particles in fine (d<1 μm) and coarse (d>1 μm) mode. The multilinear regression equations are:

$$\text{fine mode: } \gamma_m = 0.78 \cdot \gamma_c - 0.07 \cdot TC + 0.01, \tag{6}$$

$$\text{coarse mode: } \gamma_m = 0.58 \cdot \gamma_c - 0.12 \cdot TC + 0.13. \tag{7}$$

According to the equations, γ_m is in positive relationship with γ_c, while *TC* has a negative effect on the measured hygroscopic growth, as expected. The results indicate that in the fine mode γ_m can be estimated by the inorganic γ_c and the total carbon concentration, since the unknown constituents (*b*) do not play an important role (<10%) in the control of γ_m. On the other hand, in spite of the statistical relationship for coarse mode aerosol, the same conclusion cannot be drawn because of the high contribution of non-defined compounds (the share of *b* is >70%).

4. Conclusions

The hygroscopic properties of size-selected atmospheric aerosol particles were studied in 8 size intervals ranging from 62.5 nm to 16 μm at K-puszta, Hungary. Our results showed that:

1. In the fine size range ($d \leq 1$ μm):
    a. The absorbed water concentration strongly depends on the particle size, which is the consequence of differences in the chemical composition.
    b. Growth factors (both *GM* and *G*) peak in the smallest size interval, while they reach a local minimum in the range of 250–500 nm.
    c. Total carbon concentration has an important effect on the water uptake of inorganic ions. In regional background air, *TC* lowers the hygroscopicity of the particles at all *RH*s. This diminishing effect increases with increasing *RH*.
    d. The measured particle growth can be estimated by the inorganic ion and *TC* concentrations.

2. In the coarse mode (d >1 μm):
    a. The absorbed water concentration only slightly depends on the particle size.
    b. Measured growth factors (mainly above 2 μm) are underestimated by the calculated growth rates. This indicates that, in addition to the compounds analyzed in the samples, other hygroscopic constituents play an important role in the water uptake of the particles.
    c. Total carbon concentration has no statistically significant effect on the water uptake of inorganic ions.
    d. The measured particle growth cannot be estimated by the inorganic ion and the *TC* concentrations because of the important contribution of the non-determined components.

Acknowledgements—The authors are thankful for the useful comments and advices of *E. Mészáros*. The authors are also indebted to *P. Hajós* and *K. Horváth* for their help in ion chromatography. This work was supported by the National Scientific Research Fund (OTKA, project numbers: T047222 and TS049845) and by the National Program for Research and Development (NKFP, project number 3/2005). The research was done in the frame of ESF COST 633 program.

References

Aklilu, Y., Mozurkewicha, M., Prenni, A.J., Kreidenweis, S.M., Alfarra, M.R., Allan, J.D., Anlauf, K., Brook, J., Leaitch, W.R., Sharma, S., Boudries, H., Worsnop, D.R., 2006: Hygroscopicity of particles at two rural, urban influenced sites during Pacific 2001: Comparison with estimates of water uptake from particle composition. *Atmos. Environ. 40*, 2650–2661.

Alfarra, M.R., Coe, H., Allan, J.D., Bower, K.N., Boudries, H., Canagaratna, M.R., Jimenez, J.L., Jayne, J.T., Garforth, A., Li, S-M., Worsnop, D.R., 2004: Characterization of urban and rural organic particulate in the Lower Fraser Valley using two aerodyne aerosol mass spectrometers. *Atmos. Environ. 38*, 5745–5758.

Andrews, E., Larson, S.M., 1993: Effect of surfactant layers on the size changes of aerosol particles as a function of relative humidity. *Environ. Sci. Technol. 27*, 857-865.

Berner, A., 1984: Design principles of the AERAS low pressure impactor. In *Aerosols* (eds.: *B.Y.H Liu, D.Y.H Pui, H.J. Fissan*). Elsevier, Amsterdam.

Busch, B., Kandler, K., Schutz L., Neusüß, C., 2002: Hygroscopic properties and water-soluble volume fraction of atmospheric particles in the diameter range from 50nm to 3.8 μm during LACE 98. *J. Geophys. Res. 107*, D21, 8119, doi:10.1029/2000JD000228.

Chan, C.K., Kwok, C.S., Chow, A.H.L., 1997: Water activity of mixed organic and inorganic aerosols. *J. Aerosol Sci. 28*, S77-78.

Choi, M.Y., Chan, C.K., 2002: The effects of organic species on the hygroscopic behaviors of inorganic aerosols. *Environ. Sci. Technol. 36*, 2422–2428.

Clegg, S.L., Brimblecombe, P., Wexler, A.S., 1998: Thermodynamic modelling of aqueous aerosols containing electrolytes and dissolved organic compounds. *J. Phys. Chem. 102A*, 2155-2171. http://mae.ucdavis.edu/wexler/aim

Cruz, C.N., Pandis, S.N., 1997: A study of the ability of pure secondary organic aerosol to act as cloud condensation nuclei. *Atmos. Environ. 31*, 2205-2214

Cruz, C.N., Pandis, S.N., 2000: Deliquescence and hygroscopic growth of mixed inorganic–organic atmospheric aerosol. *Environ. Sci. Technol. 34*, 4313–4319.

Dick, W.D., Saxena, P., McMurry, P.H., 2000: Estimation of water uptake by organic compounds in submicron aerosols measured during the southeastern aerosol and visibility study. *J. Geophys. Res. 105*, 1471–1479.

Ferron, G.A., Karg, E., Busch, B., Heyder, J., 2005: Ambient particles at an urban, semi-urban and rural site in Central Europe: hygroscopic properties. *Atmos. Environ. 39*, 343–352.

Geresdi, I., Mészáros, E., Molnár, A., 2006: The effect of chemical composition and size distribution of aerosol particles on droplet formation and albedo of stratocumulus clouds. *Atmos. Environ. 40*, 1845-1855.

Gysel, M., Weingartner, E., Baltensperger, U., 2002: Hygroscopicity of aerosol particles at low temperatures. 2. Theoretical and experimental hygroscopic properties of laboratory generated aerosols. *Environ. Sci. Technol. 36*, 63-68.

Gysel, M., Weingartner, E., Nyeki, S., Paulsen, D., Baltensperger, U., Galambos, I., Kiss, G., 2004: Hygroscopic properties of water-soluble matter and humic-like organics in atmospheric fine aerosol. *Atmos. Chem. Phys. 4*, 35–50.

Hämeri, K., Charlson, R.J., Hansson, H-C., Jacobson, M., 1998: Hygroscopic properties of ammonium sulfate aerosol particles mixed with slightly soluble organic compound. *J. Aerosol Sci. 29*, S587-583.

Hänel, G., 1976: The properties of atmospheric aerosol particles as function of the relative humidity at thermodynamic equilibrium with the surrounding moist air. *Adv. Geophys. 19*, 73-188.

Hansson, H.C., Rood, M.J., Koloutsou-Vakakis, S., Hämeri, K., Orisini, D., Wiedensohler, A., 1998: NaCl aerosol particle hygroscopicity dependence on mixing with organic compounds. *J. Atmos. Chem. 31*, 312-346.

Hitzenberger, R., Berner, A., Giebl, H., Kromp, R., Larson, S.M., Rouc, A., Koch, A., Marischka, S., Puxbaum, H., 1999: Contribution of carbonaceous material to cloud condensation nuclei concentrations in European background (Mt. Sonnblick) and urban (Vienna) aerosols. *Atmos. Environ. 33,* 2647-2659.

Lee, C.T., Hsu, W.C., 1998: A novel method to measure aerosol water mass. *J. Aerosol Sci. 29*, 827–837.

Lee, C.T. and *Hsu, W.C.,* 2000: The measurement of liquid water mass associated with collected hygroscopic particles. *J. Aerosol Sci. 31*, 189–197.

Maßling, A., Wiedensohler, A., Busch, B., Neusüß, C., Quinn, P., Bates, T., Covert, D., 2003: Hygroscopic properties of different aerosol types over the Atlantic and Indian Oceans. *Atmos. Chem. Phys. 3,* 1377–1397.

McMurry, P.H., Stolzenburg, M.R., 1989: On the sensitivity of particle-size to relative humidity for Los Angeles aerosols. *Atmos. Environ. 23,* 497–507.

Mészáros, A., 1971: On the variation of the size distribution of large and giant atmospheric particles as a function of the relative humidity. *Tellus 23,* 436-440.

Mészáros, E., Horváth, L., 1984: Concentration and dry deposition of atmospheric sulfur and nitrogen compound in Hungary. *Atmos. Environ. 18,* 1725-1730.

Mircea, M., Facchini, M.C., Decesari, S., Fuzzi, S., Charlson, R.J., 2002: The influence of the organic aerosol component on CCN supersaturation spectra for different aerosol types. *Tellus 54B,* 74-81.

Mircea, M., Facchini, M.C., Decesari, S., Cavalli, F., Emblico, L., Fuzzi, S., Vestin, A., Rissler, J., Swietlicki, E., Frank, G., Andreae, M.O., Maenhaut, W., Rudich, Y., Artaxo, P., 2005: Importance of the organic aerosol fraction for modeling aerosol hygroscopic growth and activation: a case study in the Amazon Basin. *Atmos. Chem. Phys. 5*, 3111–3126.

Pitchford, M.L., McMurry, P.H., 1994: Relationship between measured water vapor growth and chemistry of atmospheric aerosol for Grand Canyon, Arizona, in winter 1990. *Atmos. Environ. 28*, 827-839.

Pósfai, M., Gelencsér, A., Simonics, R., Arato, K., Li, J., Hobbs, P.V., Busek, P.R., 2004: Atmospheric tar balls: particles from biomass and biofuel burning. *J. Geophys. Res. 109,* doi:10.1029/1003JD004169.

Prenni, A.J., De Mott, P.J., Kreidenweis, S.M., 2003: Water uptake of internally mixed particles containing ammonium sulphate and dicarboxylic acids. *Atmos. Environ. 37,* 4243–4251.

Rissler, J., Vestin, A., Swietlicki, E., Fisch, G., Zhou, J., Artaxo, P., Andreae, M.O., 2006: Size distribution and hygroscopic properties of aerosol particles from dry-season biomass burning in Amazonia. *Atmos. Chem. Phys. 6*, 471–491.

Saxena, P., Hildemann, L.M., McMurry, P.H., and *Seinfeld, J.H.,* 1995: Organics alter hygroscopic behavior of atmospheric particles. *J. Geophys. Res. 100,* D9, 18755-18770.

Sjogren, S., Gysel, M., Weingartner, E., Baltensperger, U., Cubison, M.J., Coe, H., Zardini, A.A., Marcolli, C., Krieger, U.K., Peter, T., 2007: Hygroscopic growth and water uptake kinetics of two-phase aerosol particles consisting of ammonium sulfate, adipic and humic acid mixtures. *J. Aerosol Sci. 38,* 157-171.

Stein, S.W., Turpin, B.J., Cai, X., Huang, P.-F., McMurry, P.H., 1994: Measurements of relative humidity-dependent bounce and density for atmospheric particles using the DMA-impactor technique. *Atmos. Environ. 28,* 9-1746.

Svenningsson, I.B., Hansonn, H.C., Wiedersohler, A., Noone, K.J., Ogren, J., Hallberg, A., Colvile, R., 1994: Hygroscopic growth of aerosol particles and its influence on nucleation scavenging in cloud: Experimental results from Kleiner Feldberg. *J. Atmos. Chem. 19,* 129-152.

Swietlicki, E., Zhou, J., Covert, D.S., Hämeri, K., Busch, B., Väkeva, M., Dusek, U., Berg, O.H., Wiedensohler, A., Aalto, P., Mkela, J., Martinsson, B.G., Papaspiropoulos, G., Mentes, B., Frank, G., Stratmann, F., 2000: Hygroscopic properties of aerosol particles in the north-eastern Atlantic during ACE-2. *Tellus 52B,* 201–227.

Temesi, D., Molnár, A., Mészáros, E., Feczkó, T., Gelencsér, A., Kiss, G., Krivácsy, Z., 2001: Size resolved chemical mass balance of aerosol particles over rural Hungary. *Atmos. Environ. 35,* 4347-4355.

Virkkula, A., Dingenen, R.V., Raes, F., Hjorth, J., 1999: Hygroscopic properties of aerosol formed by oxidation of limonene, a-pinene, and b-pinene. *J. Geophys. Res. 104,* D3, 3569-3579.

Warneck, P., 1999: *Chemistry of the Natural Atmosphere.* Academic Press, San Diego, San Francisco, New York, Boston, London, Sydney, Tokyo.

Winkler, P., Junge, C.E., 1972: The growth of atmospheric aerosol particles a function of the relative humidity, Part I. Method and measurements at different locations. *J. Recherche Atmospherique 6,* 617-638.

Zhou, J., Swietlicki, E., Berg, O.H., Aalto, P.P., Hämeri, K., Nilsson, E.D., Leck, C., 2001: Hygroscopic properties of aerosol particles over the central Arctic Ocean during summer. *J. Geophys. Res. 106,* 32111-32123.

IDŐJÁRÁS

Quarterly Journal of the Hungarian Meteorological Service
Vol. 112, No. 2, April–June 2008, pp. 83–97

Trace element analysis of airport related aerosols using SR-TXRF

Veronika Groma[1]*, János Osán[1], Szabina Török[1], Florian Meirer[2], Christina Streli[2], Peter Wobrauschek[2] and Gerald Falkenberg[3]

[1]*KFKI Atomic Energy Research Institute,*
P.O. Box 49, H-1525 Budapest, Hungary; E-mail: groma@sunsev.kfki.hu
[2]*Atominstitut der österreichischen Universitäten,*
Stadionallee 2, TU Wien, A-1020 Vienna, Austria
[3]*Hamburger Synchrotronstrahlungslabor (HASYLAB) at*
Deutsches Elektronen-Synchrotron (DESY), Notkestr. 85, 22607 Hamburg, Germany

(Manuscript received in final form May 5, 2008)

Abstract—Air quality issues of international airports are becoming more and more important due to the dynamic growth of air traffic. Fine particulate matter ($PM_{2.5}$) originating from emissions of aircrafts, ground handling vehicles, passenger related cars, and point sources is the most critical pollutant in airport areas. The sources have large temporal and spatial variation. In order to correlate the elemental composition of fine particulate matter in different size fractions to airport related sources, special instrumentation and analytical technique need to be used. A novel combination of cascade impactor sampling and total reflection X-ray flourescence (TXRF) analysis employing synchrotron radiation is presented in this paper. The method allows quantitative determination of ultra-trace amounts (pg m^{-3}) of most elements from samples collected for less than 20 min, while retaining the full size resolution of the impactor. Size-fractioned aerosol samples were collected on silicon wafers using a 7-stage May cascade impactor, close to the runway and next to the aircraft stands at Budapest Ferihegy Airport. The comparison of the size distribution of the elemental concentrations for different locations could allow us to differentiate between end-of-pipe and other emission sources. Typical elements coming from combustion processes (Zn, Pb), aircraft related emissions (Cu), as well as road salting processes (Cl) could be determined. Elements connected to crustal erosion and resuspension (Fe, Ti, Ca) had maximum concentration in the micrometer size fractions (1–4 μm). The combination of May impactor sampling and TXRF analysis described in this paper has a potential to be used in industrial/traffic processes where the time scale of the event is similar to the typical sampling durations, even using laboratory scale equipments.

Key-words: airport, air quality, fine particulate matter, trace elements, TXRF, synchrotron radiation

* Corresponding author

1. Introduction

Airport air pollution is coming to be more and more remarkable, since it shows one of the most dynamic growth in the transport sector. Large international airports operate monitoring systems (*Farias* and *ApSimon*, 2006; *Unal et al.*, 2005; *Schürmann et al.*, 2007) for continuous controlling of classical air pollutants (CO, NO_X, SO_2, O_3, PM_{10}, and $PM_{2.5}$). The statistical analyses of these long time series show that the most important pollutants which have the largest contribution to urban air quality are the nitrogen-oxides, since limiting value exceedence occurs only in NO_X concentration values (*Farias* and *ApSimon*, 2006). Whereas, measurement campaigns performed at Budapest Ferihegy International Airport during the year of 2006 show that limiting value exceedence can be detected only in particulate matter (PM_{10}) concentrations, and the only component which show higher values than downtown and suburban areas at Budapest is the fine fraction of particulate matter ($PM_{2.5}$ – particles with aerodynamic diameter smaller than 2.5 μm) (*Groma et al.*, 2007). Additionally, recent publications show that $PM_{2.5}$ causes more severe health effects than coarse particles (*Kampa* and *Castanas*, 2008).

$PM_{2.5}$ monitoring measurements were carried out using a Tapered Element Oscillating Microbalance System (TEOM) (http://www.thermo.com/eThermo/CMA/PDFs/Product/productPDF_2006.pdf) next to the runway (see *Fig. 1*), where the main particle emission sources are the starting, landing, and taxiing aircrafts, in addition to the background, since other traffic sources are far from the measurement site. Since we could determine correlation between aircrafts and $PM_{2.5}$ concentration values, it is obvious that aerosol originating from emissions of aircraft is detectable (*Bozó et al.*, 2006).

Airport related particles originate from aircraft end-of-pipe emission and erosion (brake, concrete, and tire). Moreover, not only aircrafts but also emissions of ground supporting vehicles, point sources, and passenger related cars have to be taken into account. Also, resuspension of crustal particles is a significant source. Since the most polluted sites were found to be the handling and terminal areas (apron) – where human activity is the most remarkable –, measurements capable of source apportionment are needed. Multi-element chemical analysis is one of the most adequate tools for deriving fingerprints of different sources of fine particulate matter. Also, the opportunity of short sampling time is needed, because the duration of an aircraft landing and taxiing nearby parking places is approximately 1 to 3 minutes, while touch down takes a few seconds. For this reason, development of a multielemental analytical technique for aerosol samples allowing very high temporal resolution is required, since compounds in gas phase can be measured with time resolution as low as 1 minute. This would allow a time-resolved correlation between pollutant gases and the composition of primary and secondary aerosols.

Methods allowing the analysis of individual aerosol particles on-line or from samples collected during very short time are useful for source apportionment studies. The recently developed aerosol mass spectrometers (AMS) now have the opportunity to be able to measure the size and the chemical composition of individual particles with a very high time resolution (*Takegawa et al.*, 2006), and can also be used as a monitoring instrument. The combination of time-resolved aerosol collector and computer-controlled electron probe microanalysis (CC-EPMA) of a few thousand individual particles can allow a 10 min time resolution (*Laskin et al.*, 2003). Using the AMS or CC-EPMA methods only the major chemical composition can be specified, from which the different particle types (mineral dust, sulfate, nitrate, organic) can be differentiated. Although this kind of information can be very attractive for studies of airport-related aerosols, the minor or trace elemental composition of aerosols in different size fractions is an important fingerprint of the airport related sources. The latter can be addressed by bulk trace elemental analysis of size-resolved aerosol samples collected for very short time. The aimed high size resolution as well as time resolution results in sample masses less than a microgram, which requires a very sensitive analytical method.

Total reflection X-ray fluorescence spectrometry using high flux synchrotron radiation (SR-TXRF) provides several great advantages for aerosol characterization. Because of the natural collimation of the incident beam, the high intensity of the fluorescence radiation and the low spectral background, SR-TXRF allows a non-destructive detection of trace and ultra-trace atmospheric concentrations (ng m^{-3}, pg m^{-3}) of most elements in size fractionated aerosol. Quantification and standardization of the TXRF technique is straight-forward compared to EPMA or AMS.

Recent investigations present many studies about aerosol measurement methods which have high time resolution and low detection limits. These developments are usually based on size fractionated aerosol sampling combined with TXRF analyses. Results show that they are capable for determination of specific elements, source identification, and fingerprint analysis based on samples collected within hours (*Dudzinska-Huczuk* and *Bolalek*, 2007; *Lammel et al.,* 2007). Whereas, a great disadvantage of these methods lies in the necessity of a pretreatment of the sample carriers used in TXRF analysis in some cases (*John et al.*, 2001). Moreover, higher time and size resolution is needed to study atmospheric processes having characteristic times in the range of hours (*Lammel et al.*, 2007). Since our aim was to study even shorter environmental processes, we needed to develop a method which has better time resolution characteristics. Since the risk of contamination is higher at lower amounts (ng) of samples, the applied technique should be devoid of this problem. Sampling with May impactor combined with SR-TXRF seemed to be a good alternative, since this technique does not need any pretreatment of

samples, and also non-destructive, which allows one to perform further analysis on the collected aerosols.

The aim of this study is (i) to introduce an aerosol analysis method which has potential to use in industrial/traffic processes where the time scale of the event is similar to the typical sampling duration, and (ii) to present its suitability for trace element analysis of airport related aerosols.

2. *Materials and methods*

2.1. Sampling

Aerosol samples were collected in the inside area of Budapest Ferihegy Airport. The airport is located 15 km south-east from the city center of Budapest. A highway with approximately 50,000 cars day^{-1} traffic is located 2 km far from the airport area. The potential measurement sites inside the airport were limited, because movements at the airport area were strictly regulated. Hence, it was not possible to go closer to the runway than 150 meters. To overcome the security problems and reduce influence of road transfer, measurements were performed near the runway and next to terminal buildings (apron) (see *Fig. 1*).

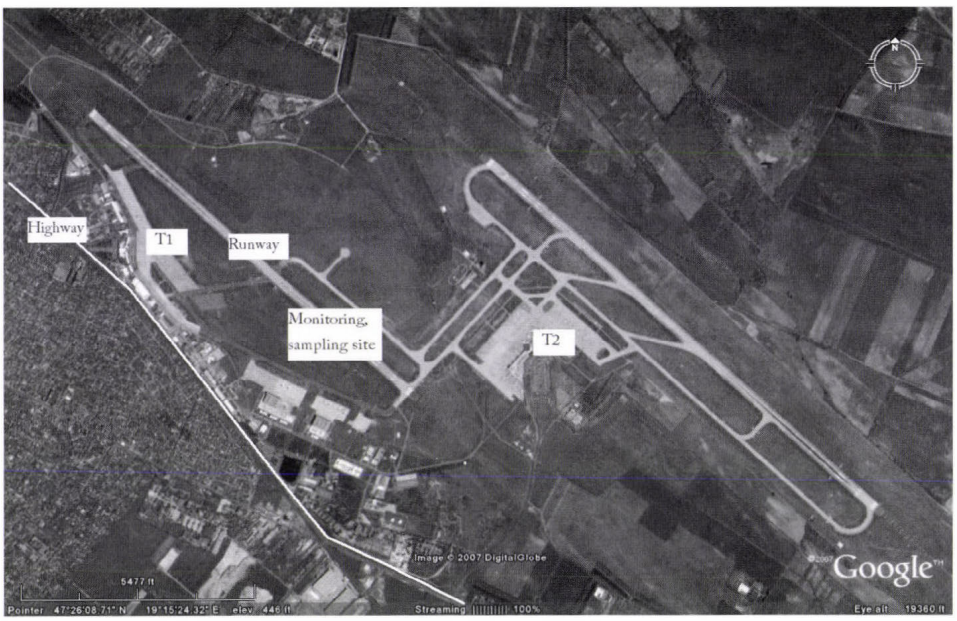

Fig. 1. Measurement sites at Budapest Ferihegy Airport.

First, samples were collected on 20×20 mm^2 silicon wafers using a 7-stage May cascade impactor (*May*, 1975). The May impactor has aerodynamic cut-off diameters of 16, 8, 4, 2, 1, 0.5, 0.25 μm for stages 1–7, respectively, at 20 l min^{-1} sampling flow rate. The sampling duration took 1 (for stage 7), 5 (for stage 6), 10 (for stage 5), and 20 minutes (for stage 4) to obtain the best loading of particles on the impacted strips. Since in this study we aim to investigate the fine aerosol fraction only, aerosol collection was performed only for the above specified four stages (4 to 7). The May impactor has an impacting slit at each stage, and thus the aerosols collected on a silicon substrate show a pattern of a thin line with approximate dimensions of 20 mm × 0.3 mm. To be able to calculate concentration values for each trace element, an internal standard, a Cr strip with a known mass was placed on the Si wafers exactly at the same position as particles from the air sample, prior to collection of particulate matter on the Si carriers. Two sample sets were collected on January 12, 2006 at the runway and Terminal 2 (high traffic: 8 aircraft movements during sampling time), and one at Terminal 1 (low traffic: 1 aircraft movement during sampling time) on January 15, 2006 (hereafter, T2 and T1, respectively). The last sampling day was a Sunday with much lower traffic in the city of Budapest.

Ionic compounds were measured in order to obtain daytime and nighttime averages of sulfate concentrations in $PM_{2.5}$, samples were collected on 1 μm pore-size Teflon filters for 12 h at the terraces of terminal buildings. The cyclone used for the fine aerosol sampling had a cut-off diameter of 2.5 μm at 10 l min^{-1} flow rate. The total sampled air volume was approximately 7 m^3 for all samples. The 12-hour average concentrations of sulfate were measured using ion chromatography (IC), after leaching the filter samples in water.

2.2. Multielemental analysis

Measurements were performed at HASYLAB Beamline L using a total-reflection X-ray fluorescence vacuum chamber (*Streli et al.*, 2005). An automatic sample loader (*Meirer et al.*, 2006) was installed to establish the opportunity to measure 8 samples consecutively without the necessity to close the beam shutter and open the vacuum chamber, resulting significant time saving during the beam time. A special sample holder was used to mount the 20×20 mm^2 Si wafer pieces with the aerosol samples collected in strip form. The synchrotron radiation energy was adjusted to 18.4 keV by means of the NiC multilayer monochromator. The SR beam had a vertical dimension of 1.4 mm and a horizontal dimension of 0.2 mm.

A Vortex Radiant Silicon Drift Detector (SDD) in use was equipped with a special collimator with a 1.5 mm wide slit made of Mo, in order to fit to the geometry of the impacted aerosol samples. As X-ray photons emerging from the total 20 mm length of the aerosol strip could not be detected using the SDD applied, the homogeneity of the aerosol deposition was tested. For the test scans,

the sample strip and the collimator slit was perpendicular to the X-ray beam, therefore, only 1.4 mm section of the sample strip was excited. The vertical scans were performed by moving the sample–detector system relative to the position of the beam using a stepping motor. The step size was set to 1 mm, and the individual spectra were collected for 3 s. Measurements with the new collimator resulted in excellent reproducibility of the individual scan steps. The interpretation is clearly a shielding of the off-lier contaminants as the slit prevented their detection and the geometry of the detector collimator fit to the sample. The measurements aiming the determination of the elemental concentrations were carried out applying the SR beam parallel to the sample strip. The position of the sample strip was determined using vertical scans with 0.2 mm step size. Individual spectra were collected at the strip positions for 100 s. The net characteristic X-ray intensities of the elements were calculated by evaluating the spectra by non-linear least-squares fitting using the AXIL program (*Vekemans et al.*, 1994). In order to calculate the relative sensitivity curve of the setup, 30 nl of a multielement standard solution (11355 Multi Element Standard IV, Merck) containing 1 ng of each element was pipetted onto a Si wafer and measured by SR-TXRF.

3. Results and discussion

3.1. Sample homogeneity

Samples were collected directly on Si wafers containing 5.75 ng Cr in a 300 μm wide strip in the middle centerline of the wafers. As the geometry of the Cr strip was chosen to be similar to that of the deposited aerosol particles, Cr could be efficiently used as internal standard for the SR-TXRF measurements. The standards were provided by the Research Institute for Technical Physics and Materials Science (Budapest, Hungary) (*Watjen et al.*, 2000). The important issue is to make sure that the measured 6 mm sections of the aerosol strip are representative for the total length and thus for the calculation of the total mass deposited here. Only if this is proven, the extrapolation from the mass calculated for 6 mm to the total mass deposition is permitted. The total mass deposited represents the aerosol concentration (ng m^{-3}) in the collected air volume. For this purpose 18 mm of the existing 20 mm strips were measured successively by scanning 3 × 6 mm along the strip. Results shown in *Fig. 2* demonstrate that the Fe intensities normalized to ring current vary within 10% relative standard deviation during the three scans, supporting the proposed extrapolation.

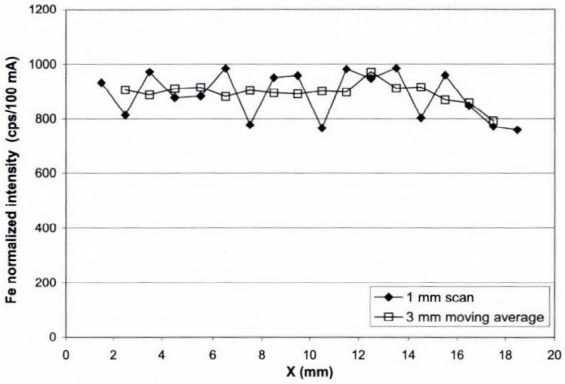

Fig. 2. Results of homogeneity test of impacted aerosol strip.

3.2. Elemental analyses

Long term measurement data showed slight differences between PM_{10} and $PM_{2.5}$ concentrations (*Groma et al.*, 2007). For this reason size fractioned aerosol analyses were only done on the smaller sized particles (0.25–4 μm aerodynamic diameter). Also, larger particles occur in smaller number concentration (particles m^{-3}) naturally, requiring longer sampling time, which does not make any sense on the time-scale of aircraft movements. May impactor sample collection combined with SR-TXRF analysis has the opportunity to calculate elemental concentrations from extremely small sampling volumes. Detection limits achieved for 20-minute sampling time are ranging from ng m^{-3} for the light elements (Al, Si) to pg m^{-3} for the medium *Z* elements like Rb and Sr in the present matrix (see *Table 1*). The detection limits were calculated for 100 s measuring live time and 100 mA ring current.

Table 1. Detection limits for each element detected in aerosol particles collected at airport sites

Element	Detection limit (pg m^{-3})
S	451.3
Cl	282.8
K	107.9
Ca	68.3
Ti	39.9
Cr	23.4
Fe	13.3
Cu	4.6
Zn	3.4
Se	2.4
Br	2.3
Sr	3.6
Pb	5.8

The concentrations of the elements in the samples were calculated based on SR-TXRF spectra collected for 100 s, using the Cr strip as internal standard. A typical spectrum is presented in *Fig. 3*.

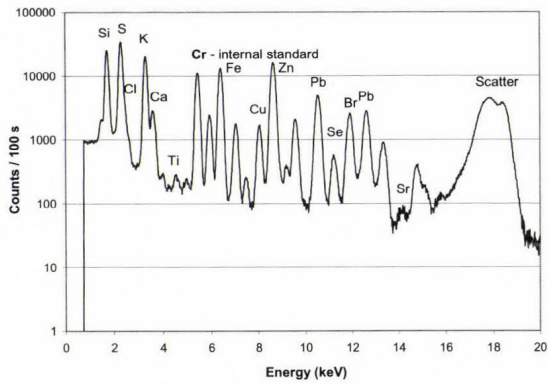

Fig. 3. Typical SR-TXRF spectrum of an aerosol sample collected at the airport, 0.5–1 μm size fraction.

The SR-TXRF measurement results of airport related aerosols sampled by May impactor are presented in *Fig. 4*. Since aerosols were collected in 4 different size fractions at 3 different sites, measurement results for 12 samples are presented here. Each diagram is relevant for one of the elements studied (S, Cl, K, Ca, Ti, Fe, Cu, Zn, Se, Br, Sr, Pb). Each column is relevant for a measurement site: runway, T2 – high traffic (85%) and T1 – low traffic (15%), respectively. Size distribution of concentrations for a specific element is presented within the columns. Diagrams are scaled to the maximum values of the different elements. Measurement results shown in *Fig. 4a–l* confirm facts which were previously expected for typical suburban areas, besides results which show specialties of airport related aerosols. Aerosols originate from long range transport, city plume, and local sources. Local sources show large variability in the airport, since aircrafts, ground supporting vehicles, and also passenger cars have to be taken into account. The emission characteristics are all different, some of them are well known, but some – especially aircraft related – particulates chemical composition is still unknown.

Onsite measurements were recently performed by NASA to improve air quality emission inventories (*Aviation Particle Emissions Workshop*, 2004). These results are very well detailed, but the instrumentation requirement is huge, and no trace element composition analysis can be performed. It follows that the combination of impactor sampling and SR-TXRF analysis presented in this paper provides complementary information.

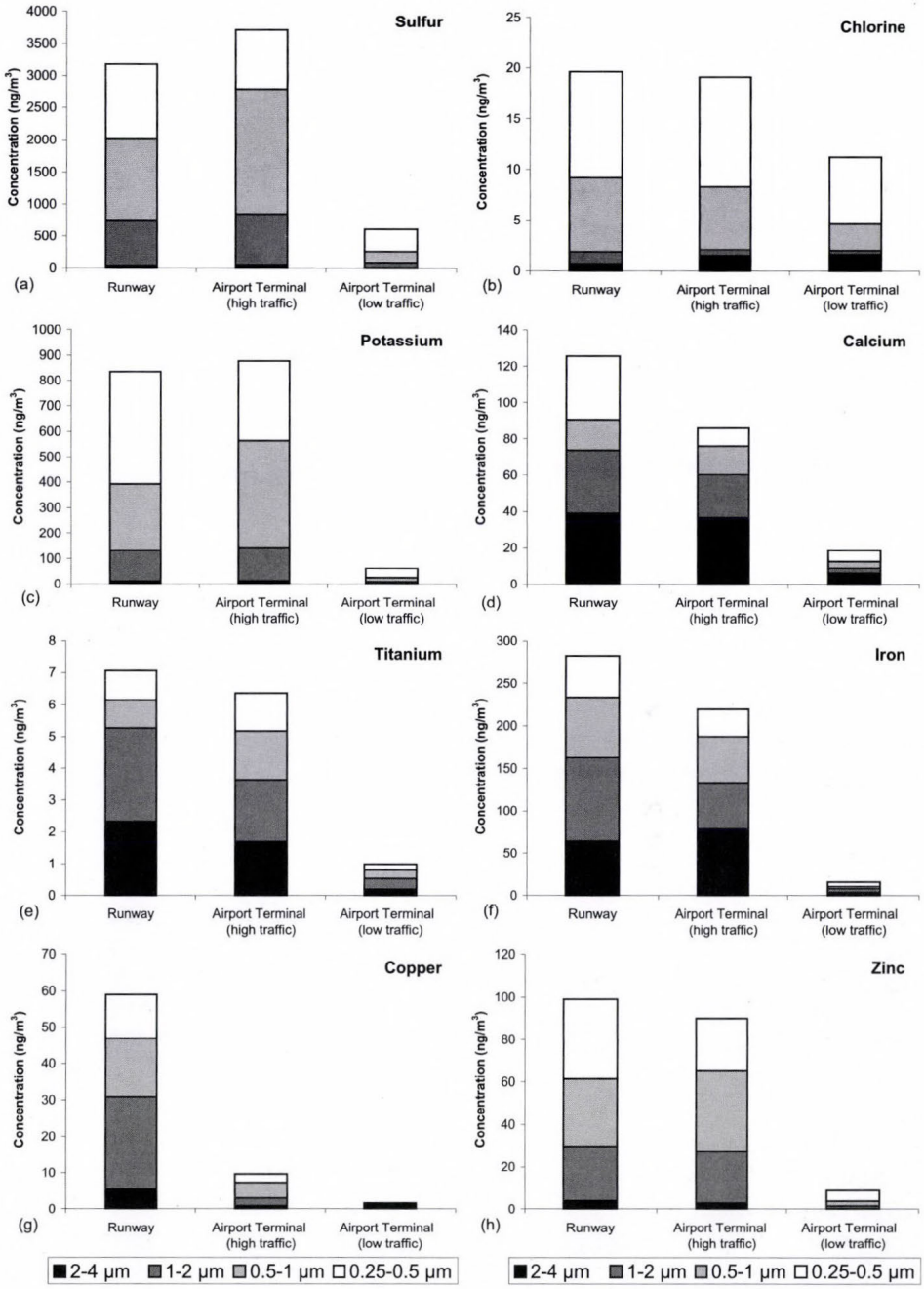

Fig. 4. Size distribution of elemental concentrations at different sites.

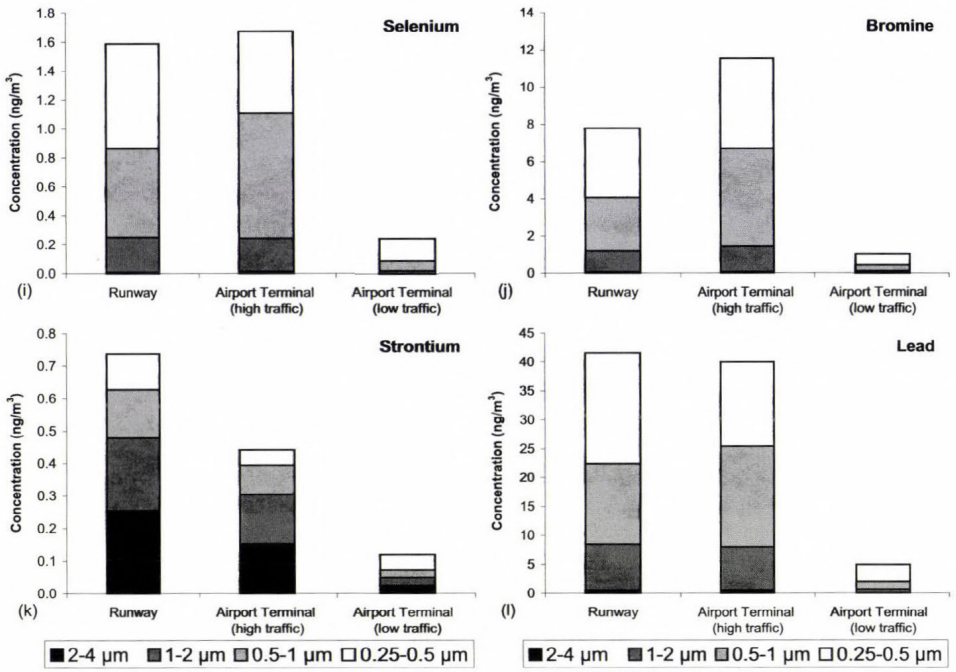

Fig. 4 (continued). Size distribution of elemental concentrations at different sites.

Not only combustion processes, but also resuspension, erosion, and formation of secondary aerosols (which can be classified in typical size fractions) contribute to the ambient particulate concentration. Therefore, measurement results can be discussed in 3 different aspects: (i) size distribution, (ii) magnitude of concentration values at different sites, and (iii) typical elements at different sites. It is obvious to see that concentrations of all elements measured at runway and terminal building with larger traffic (T2) are much higher than values at the other terminal with lower traffic (T1). This is due to the different number of air as well as ground vehicle movements around the sampling sites. Sample collections at the runway and T2 (just after each other) were done during one of the largest aircraft traffic peaks (around 1 p.m.), while sampling at T1 was performed during really small number of vehicle movements. Airport traffic does not only mean the movements of aircrafts, but also ground supporting and passenger cars which both show correlation with aircraft movements. To be able to determine the origin of the aerosol, samples collected at different sites need to be compared. Since the source properties at terminal buildings are complex (large temporal and spatial variation), it is not possible to determine the origin of particles from their chemical composition.

Results from terminal building compared to results from the runway allow one to differentiate between the sources.

It is well-known that sulfate is dominant in smaller size fractions. According to *Kerminen et al.* (2004), the size distribution of sulfate shows a maximum at around 0.3 μm for rural and around 0.7 μm for urban aerosols, based on measurements at several European sites. Previous studies of Hungarian background aerosol have even revealed that the preferred modal diameter of sulfate compounds is smaller in the summer than in the winter (*Mészáros et al.*, 1997). As it can be seen in Fig. 4a, the shape of the size distribution is similar to that observed by impactor sampling and IC measurements reported in the literature (*Kerminen et al.*, 2004; *Mészáros et al.*, 1997). The highest sulfur concentration obtained by SR-TXRF is in the 0.5–1 μm fraction at the runway and at T2, and in the 0.25–0.5 μm fraction at T1. It means that the size distribution of sulfur has a more rural characteristic for low traffic conditions, and more urban at sites influenced by high traffic.

Significant amount of Cl was found to be present in the largest size fraction studied (2–4 μm). Besides long-range transport of sea salt, chlorine also originates from the salt used for preventing ice formation on roads during winter time. The SR-TXRF results are in accordance with this, since the decrease of the traffic intensity at the airport has less influence on the concentrations of Cl than other elements (see *Fig. 4b*).

Ca, Fe, and Ti show similar size distribution at the three locations (see *Figs. 4d, 4e, 4f*). Also, the total concentration values of these elements have similar ratio among the three sites. This means that the source of particles containing these elements must be the same. Since these elements dominate in larger particulates, one can say that they probably originate from resuspension (by movements of vehicles and the blowing effect of the aircraft engine).

Zinc and lead (see *Figs. 4h, 4l*) are usually connected to combustion processes in the engine (*Tesseraux*, 2004). Traffic related particles containing these elements usually occur in fine aerosols, which is in good agreement with our results. Because concentration values of these elements show similar magnitudes: high at high traffic periods and low at the time of low traffic, but no significant difference could be seen at the runway and T2, one can say that particulates containing these elements should originate from the airport related ground supporting vechicles as well as from the city traffic, transported to airport area.

Significant differences between apron and runway areas are in copper concentration values (see *Fig. 4g*). Copper rich particles probably originate from aircraft brake pad erosion. No other studies have been done connected to the erosion during aircraft landing, which means further investigations are needed to be done on this subject.

High concentration values of potassium usually occur near wood-burning emission sources which cannot be found inside, but probably somewhere

outside, near the airport area. This is confirmed by the fact that sulfur has a really similar size distribution to potassium (see *Figs. 4a, 4c*), which is also connected to wood-burning processes in previous studies (*Osán et al.*, 2002).

Since strontium is chemical substituting element for calcium, the size distribution and Sr/Ca ratio at different sampling sites should be the same. Although Sr was found to be present at sub-ng m^{-3} concentration levels (see *Figs. 4k* and *4d*), the present measurement results confirm these assumptions. This very good correlation between Sr and Ca concentrations in all size ranges clearly shows the suitability of SR-TXRF for trace element analysis of aerosol samples.

Selenium and bromine rich particles were found to be dominant in the submicrometer size fractions (see *Figs. 4i, 4j*), therefore, these trace elements can be connected to the combusted fuels used either in air or in ground traffic. The detection of this small quantity in these small size-fractions confirms the fact that this method opens up new opportunities in aerosol analysis research.

3.3. Comparison of IC and SR-TXRF measurements

Since the sulfate content of the $PM_{2.5}$ aerosol at the airport could be measured by IC from 12-hour filter sampling on the same day, it is worth to compare the results obtained by the two techniques. SR-TXRF sulfate concentrations were calculated from stoichiometry based on the sum of the sulfur concentrations for the size fractions in the 0.25–2 μm range.

$PM_{2.5}$ sampling on Teflon filters was done on T2 terminal building during both days, when aerosol collection was performed with the May impactor. Since a large air volume is needed for the IC analyses, the samples were collected for 12 hours. Because the meteorological and traffic conditions are not stationary, it is not trivial to compare the results of these samples with those from SR-TXRF analyses, which are samples collected for much shorter time. *Table 2* shows the results of sulfate concentrations obtained by ion chromatography and SR-TXRF.

Comparing IC and SR-TXRF measurement results for samples originating from the same site during a larger airport traffic volume period shows similar values (less than 20% difference). Also, SR-TXRF results at the runway are in the same magnitude of the ones mentioned above. However, sulfate concentration of aerosol particles collected for 12 hours and analyzed by IC is higher than those measured by SR-TXRF, which should be explained by the fact that a significant sulfate mass can be present in ultrafine particles smaller than 0.25 μm. Also, the short time May impactor sample collection was not performed during the highest traffic period (inside and outside the airport). This also confirms the fact, that long range transport is one of the most important sources of aerosols containing sulfate, besides the local emission and formation effects. To study the contribution of these processes further measurements are needed.

The use of the recently developed ambient ion monitor (http:// www.urgcorp.com/systems/pdf/9000.pdf) that allows IC measurements of ionic compounds in $PM_{2.5}$ at a time resolution of 15 minutes would lead to a more accurate comparison between IC and SR-TXRF results. However, this new IC system is still not capable for providing size-fractionated information.

Table 2. Differences in sulfate concentrations analyzed by IC and SR-TXRF

Sampling site, method	**Runway SR-TXRF**	**T2, SR-TXRF**	**T2, IC**
Concentration (ng m^{-3})	9,500	11,100	13,500

4. Summary and conclusion

Aerosol collection with May impactor combined with the SR-TXRF analytical method could be efficiently used to study atmospheric processes on the time scale of minutes. The sampling and trace element analysis were performed at airport sites near sources which show high spatial and temporal variability. Measurements and trace element analysis at airport sites with such high size resolution have never been done before. We could determine typical aircraft originated particles from these extremely small sampling volumes.

Since the concentration of $PM_{2.5}$ found to be the most critical at airport sites, the aim of our measurements was to determine the airport related aerosol particles. Typical elements of combustion processes like zinc and lead could be determined as well as special, aircraft related particles, namely high copper concentrations were detected near the runway, which is due to aircraft brake erosion. Size fractioned sampling allowed us to sort out particles from not airport related combustion processes, since, for example, due to resuspension, typical aerosols in larger size fractions (Ca, Fe, Ti) can be shown. Also, from the comparison of concentration magnitudes at different sites, we could identify elements originating from wood burning processes like potassium and sulfur, which are connected to atmospheric transport.

Low detection limits (in the range of pg m^{-3}) could be achieved from 20 minutes sampling time thanks to the excellent properties of synchrotron radiation. This short time collection allows to study temporal variation of elemental concentrations in size-fractioned aerosols. SR-TXRF measurements have proven the fact that the most important elements occur in concentrations above detection limits. By choosing the most adequate size and time resolution to that samples, the method prospects to use laboratory TXRF instrumentation also. The aim of our further developments is to establish an instrumentation using the above performed methods which can be used in monitoring measurements.

Acknowledgements—This work was supported by the Jedlik Ányos Programme of the National Office for Research and Technology through contract No. 3/019/2005 and by the European Community - Research Infrastructure Action under the FP6 "Structuring the European Research Area" Programme (through the Integrated Infrastructure Initiative "Integrating Activity on Synchrotron and Free Electron Laser Science") Contract RII3-CT-2004-506008.

The support of the Hungarian Scientific Research Fund (OTKA T049581) and the Austrian–Hungarian Action Foundation (62öu10) are also appreciated. The authors would like to thank the staff of Budapest Airport Zrt. for their help during sampling at the airport.

References

Aviation Particle Emissions Workshop, 2004: Proceedings of a conference sponsored by the Ultra-Efficient Engine Technology (UEET) Project under the Vehicle Systems Program (VSP) of the National Aeronautics and Space Administration (NASA). Cleveland, Ohio, November 18-19, 2004. National Aeronautics and Space Administration, Glenn Research Center, NASA/CP—2004-213398.

Bozó, L., Czitrovszky, A., Alföldy, B., Osán, J., Groma, V., Ferenczi, Z., Labancz, K., Nagy, A., Steib, R., Kalocsainé, M., Récsei, I., Polay, P., 2006: Environmental monitoring system of airport traffic (in Hungarian). Progress report of the Ányos Jedlik Project No. 3/019/2005, October 2006, AEKI-SKL-2006-204-01-01-0. KFKI, Budapest.

Dudzinska-Huczuk, B., Bolalek, J., 2007: Particulate selenium in the Baltic Sea atmosphere. *Water Air Soil Poll. 179*, 29–41.

Farias, F., ApSimon, H., 2006: Relative contributions from traffic and aircraft NO_x emissions to exposure in West London. *Environ. Modell. Softw. 21*, 477–485.

Groma, V., Alföldy, B., Osán, J., Kugler, S., Kalocsai, M., 2007: Impact of the airport related traffic on the urban particulate pollution. *Proceeding of European Aerosol Conference*. 9-14 Sept. 2007, Salzburg, Austria.

John, A.C., Kuhlbusch, T.A.J., Fissan, H., Schmidt, K.-G., 2001: Size-fractioned sampling and chemical analysis by total-reflection X-ray flourescence spectrometry of PM_x in ambient air and emissions. *Spectrochim. Acta B, 56*, 2137–2146.

Kampa, M., Castanas, E., 2008: Human health effects of air pollution. *Environ. Pollut. 151*, 362–367.

Kerminen, V.-M., Hillamo, R., Teinilä, K., Pakkanen, T., Allegrini, I., Sparapani, R., 2004: Ion balances of size-resolved tropospheric aerosol samples: implications for the acidity and atmospheric processing of aerosols. *Atmos. Environ. 35*, 5255–5265.

Lammel, G., Baumgardner, D.G., Fittschen, U.E.A., Peschel, B., 2007: Evolution of anthropogenic aerosols in the coastal town of Salina Cruz, Mexico: Part III size-segregated elemental composition analysed by total-reflection X-ray fluorescence spectrometry. *Int. J. Environ. An. Ch. 87*, 659–672.

Laskin, A., Iedema, M.J., Cowin, J.P., 2003: Time-Resolved Aerosol Collector for CCSEM/EDX Single Particle Analysis. *Aerosol Sci. Tech. 37*, 246–260.

May, K.R., 1975: An "ultimate" cascade impactor for aerosol assessment. *J. Aerosol Sci. 6*, 413–416.

Meirer, F., Streli, C., Wobrauschek, P., Zoeger, N., Jokubonis, C., Pepponi, G., Falkenberg, G., Osan, J., Torok, S., Groma, V., Fittschen, U., Broekaert, J., Mihucz, V.G., Zaray, G., Czech, V., Hofstaetter, J., Roschger, P., Simon, R., 2006: Recent results of the ATI X-Ray group with SR-TXRF, *XRF Newsletter*.

Mészáros, E., Barcza, T., Gelencsér, A., Hlavay, J., Kiss, G., Krivácsy, Z., Molnár, A., Polyák, K., 1997: Size distributions of inorganic and organic species in the atmospheric aerosol in Hungary. *J. Aerosol Sci. 28*, 1163–1175.

Osán, J., Alföldy, B., Török, S., Van Grieken, R., 2002: Characterisation of wood combustion particles using electron probe microanalysis. *Atmos. Environ. 36*, 2207–2214.

Schürmann, G., Schäfer, K., Jahn, C., Hoffmann, H., Bauerfeind, M., Fleuti, E., Rappenglück, B., 2007: The impact of NO_x, CO and VOC emissions on the air quality of Zurich airport. *Atmos. Environ. 41*, 103–118.

Streli, C., Pepponi, G., Wobrauschek, P., Jokubonis, C., Falkenberg, G., Zaray, G., 2005: A new SR-TXRF vacuum chamber for ultra-trace analysis at HASYLAB, Beamline L. *X-Ray Spectrom. 34*, 451–455.

Takegawa, N., Miyakawa, T., Kondo, Y., Jimenez, J.L., Zhang, Q., Worsnop, D.R., Fukuda, M., 2006: Seasonal and diurnal variations of submicron organic aerosol in Tokyo observed using the Aerodyne aerosol mass spectrometer. *J. Geophys. Res.-Atmos. 111*, Art. No. D11206.

Tesseraux, I., 2004: Risk factors of jet fuel combustion products. *Toxicology Letters 149*, 295–300.

Unal, A., Hu, Y., Chang, M.E., Odman, M.T., Russell, A.G., 2005: Airport related emissions and impacts on air quality: Application to the Atlanta International Airport. *Atmos. Environ. 39*, 5787–5798.

Vekemans, B., Janssens, K., Vincze, L., Adams, F., Van Espen, P., 1994: Analysis of X-ray spectra by iterative least squares (AXIL): New developments. *X-Ray Spectrom. 23*, 278–285.

Watjen, U., Bárson,y I., Dücső, C., 2000: A Novel Micro-Structured Reference Material for Ion and X-Ray Microbeam Analysis. *Mikrochim. Acta 132*, 521–525.

IDŐJÁRÁS

Quarterly Journal of the Hungarian Meteorological Service
Vol. 112, No. 2, April–June 2008, pp. 99–112

Airport (Budapest Ferihegy – Hungary) air quality analysis using the EDMS modeling system. Part I. Model development and testing

Roland Steib[1], **Krisztina Labancz**[1], **Zita Ferenczi**[1] and **Bálint Alföldy**[2]

[1]*Hungarian Meteorological Service, P.O. Box 39, H-1675 Budapest, Hungary*
[2]*Hungarian Academy of Sciences KFKI Atomic Energy Research Institute, P.O. Box 49, H-1525 Budapest, Hungary*
E-mails: steib.r@met.hu, ferenczi.z@met.hu, labancz.k@met.hu, alfi@sunserv.kfki.hu

(Manuscript received in final form May 5, 2008)

Abstract—This paper presents an application of the EDMS dispersion modeling system to airport air quality calculations. The EDMS system is a combined emissions and dispersion model which can be used to produce an inventory of emissions generated at Budapest Ferihegy Airport, as well as to calculate pollutant concentrations on and around the airport. Calculated yearly average NO_x and CO concentration distributions over the area of the airport are presented. Calculated hourly average NO_x and CO concentration values are compared with observed air pollution concentrations and meteorological data, which were measured during three measurement campaigns held in the area of Budapest Ferihegy Airport.

Key-words: airport air quality, dispersion modeling, EDMS modeling system

1. Introduction

Aviation has experienced rapid expansion as the world economy has grown, and this has produced a number of major environmental challenges (*Britter*, 2007). As the contribution to urban air pollution from road emissions is steadily reducing in cities of European countries, other emission sources are becoming comparatively more relevant. The contribution to air pollution levels from emissions produced by the operation of airports located close to cities is one example in this respect. This phenomenon is accentuated due to urban settlement dynamics resulting in increases in the number of people exposed either living or working around these facilities and expansion wishes of airport operators to cope with forecasted increases in air traffic demand.

There are a number of widely used operational atmospheric dispersion models applied to airports (*Barrett* and *Britter*, 2007). In the early 2000's, a model intercomparison was executed in the framework of the Project for the Sustainable Development of Heathrow (*Department for Transport, U.K.*, 2006). Three models addressing local air quality at airports were compared with monitored air quality data and each other: (i) ADMS-Airport, based on the ADMS-Urban, a quasi-Gaussian dispersion model nested within a trajectory model (*Carruthers et al.*, 1994, 2007); (ii) LASPORT, based on the LASAT Lagrangian dispersion model (*Janicke et al.*, 2007); (iii) EDMS, based on the AERMOD quasi-Gaussian regulatory-type dispersion model (*CSSI, Inc.*, 2004). Apart from this study, in 2005 the EUROCONTROL initiated the ALAQS project to develop a European methodology and model (ALAQS-AV) to assess aviation's contribution to the degradation of the local air quality in surroundings of airports (*EUROCONTROL*, 2005).

Budapest Ferihegy Airport is not one of the internationally registered busiest airports, but the volume expanding of its traffic requires to be aware of its impact on air quality. By the recommendation of EEA (European Environment Agency), in case an airport has more than 100 thousands LTO cycles (landing, take-off, and taxi) per year, the airport becomes an important air pollution source in the national balance. The traffic at the airport is near to this limit. Especially in the summer period a large number of charter flights can increase the traffic significantly.

In 2005, a new project started to determine the air pollution situation at Budapest Ferihegy Airport, combining the results of measurements and model calculations. Airport related particles originate from aircraft emissions and erosion (brake and tire), moreover, emissions of ground supporting vehicles, point sources, and passanger related cars as well as resuspension of particles had to be taken into account. In the joint research work, the EDMS air quality modeling system was adapted and developed at the Hungarian Meteorological Service (HMS), while three measurement campaigns were performed on the area of Budapest Ferihegy Airport by the Hungarian Research Institute of Physics. The EDMS model system was chosen on the base of studies presented by recent investigations, because the AERMOD dispersion model has been earlier adapted at the HMS including a newly developed terrain preprocessor. During the measuring campaigns, concentration of numerous air pollutants were detected including usual pollutants as nitrogen oxides and carbon-monoxide, as well as rarely observed pollutants as tire and soot, which are characteristic of air traffic. Multi-element chemical analysis were done with high size resolution for deriving fingerprints of different sources of airport related particles.

This paper presents the first results of the EDMS modeling system, compared to the measured data during three short time measuring campaigns. Section 2 describes the model and its required input data, in Section 3 the modeled yearly averages of the concentration of NO_x and CO are presented, and Section 4 presents the comparison of the modeled and observed NO_x and CO data.

2. *The EDMS modeling system*

2.1. The EDMS model

The EDMS (Emissions and Dispersion Modeling System) has been considered a preferred model for airport air quality analysis. The modeling system EDMS was developed in the mid-1980s as a complex source microcomputer model designed to assess the air quality impacts of proposed airport development projects. EDMS is a combined emissions and dispersion model for assessing air quality at the airports. The model is used to produce an inventory of emissions generated by sources on and around the airport or air base, and to calculate pollutant concentrations in these environments. The policy statement is intended to ensure consistency and quality of analysis performed to assess the air quality impacts of airport emission sources for purposes of complying with the National Environmental Policy Act.

The previous version of EDMS (Version 3.23) used CALINE3 and PAL2 models for atmospheric dispersion. In the first quarter of 2001, CALINE3 and PAL2 were replaced by AERMOD quasi-Gaussian dispersion model and its supporting weather and terrain processors, AERMET and AERMAP in Version 4.0 of EDMS. AERMOD has better characterization of the planetary boundary layer (*Steib*, 2006) and allows dispersion to be accomplished using continuous functions rather than with discrete stability classes that do not change with height. In the convective boundary layer a good approximation to the probability density function (PDF) is the superposition of two Gaussian distributions (*Baerentsen* and *Berkowicz*, 1984; *Weil*, 1988), so instead of a Gaussian distribution for both the horizontal and vertical directions, AERMOD uses a bi-Gaussian probability density function, p_w, to characterize the dispersion in the vertical direction (*Cimorelli et al.*, 2004):

$$p_w = \frac{\lambda_1}{\sqrt{2\pi}\sigma_{w1}} \exp\left(-\frac{(w-\overline{w_1})^2}{2\sigma_{w1}^2}\right) + \frac{\lambda_2}{\sqrt{2\pi}\sigma_{w2}} \exp\left(-\frac{(w-\overline{w_1})^2}{2\sigma_{w1}^2}\right), \qquad (1)$$

where λ_1 and λ_2 are weighting coefficients for the two distributions with $\lambda_1 + \lambda_2 = 1$ (the subscripts 1 and 2 refer to the updraft and downdraft distributions, respectively). The parameters of the probability density function (w_1, w_2, σ_{w1}, σ_{w2}, λ_1, λ_2) are functions of σ_w (the "total" or overall root mean square of vertical turbulent velocity). AERMOD also incorporates a new, simple method to model flow and dispersion in complex terrain.

The EDMS version used for this study is EDMS Version 4.5. The model can calculate emission inventories for the following pollutants: CO, NO_x, SO_x, total hydrocarbons (THC), non-methane hydrocarbons (NMHC), volatile organic compounds (VOC), $PM_{2.5}$, and PM_{10}.

At the HMS, the AERMOD model system was adapted first (*Steib* and *Labancz*, 2005). Because of the input data file formats required for AERMET and AERMAP are not available at HMS, new pre-processors were developed for preparing the input files for the dispersion model. The MM5 numerical weather prediction model analysis files are used as meteorological input of AERMOD. After successful setting up of AERMOD, the adaptation of EDMS was not too difficult work. The input files needed for AERMOD were generated by the EDMS model, then AERMOD was run on another computer because of the large memory needs of the dispersion model. *Fig. 1* shows the architecture of the EDMS modeling system.

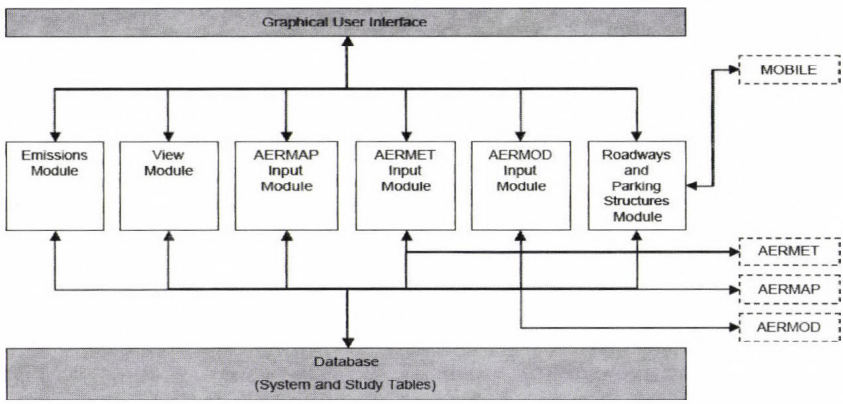

Fig. 1. EDMS system architecture and components.

2.2. EDMS input required

EDMS generates input files for use with the AERMOD dispersion model. Since EDMS is a model specifically developed for use at airports, the inputs relate directly to the placement of aircraft and other source activity and movement on the airport. Data input includes:

1) Creation and specification of
   - runways,
   - queues,
   - taxiways,
   - buildings, and
   - gates.
2) Emission data of
   - aircraft activity,
   - ground support equipment,
   - on-road vehicles,

- parking facilities,
- stationary sources, and
- training fires.

Aircraft activity is expressed in landing-takeoff (LTO) cycles. Each LTO consists of taxiing, queuing, takeoff, climb out, approach, and landing. There is no provision to specify arrival numbers and departure numbers independently of each other. EDMS contains default aircraft-specific data relating to the emissions:

1) Times in mode (TIMs) are the durations per LTO cycle that an aircraft spends in each of the four modes of aircraft operation. Takeoff, climb out, approach, and landing mode TIMs are aircraft-specific in EDMS.
2) Ground support equipments (GSE) are made to be based on aircraft type with an operating time associated with each aircraft LTO cycle.
3) Aircrafts are assigned to an unlimited number of taxiways and runways.
4) Engine emission factors are aircraft-specific.

2.3. Emission data

The dispersion model calculates concentrations for 1 hour periods, and all source types can vary hour by hour in their activity or strength. Therefore, EDMS uses operational profiles which are based on the concept of peak activity. A peak hour, day, or month is defined as that at which the most or maximum activity occurs. Peak activity is represented by a proportional factor of 1 (signifying maximum activity).

In our study three categories are defined for the aircrafts – light, medium, heavy – in accordance with the International Civil Aviation Organization (ICAO) scheme. Each category is represented by the aircraft-type most frequently operated at Ferihegy Airport (Socata Tampico – light, Boeing 737 – medium, Boeing 767 – heavy). All aircrafts are replaced by the appropriate defined aircraft with its default specific data. Hourly, daily, and monthly operational profiles are also calculated for the three defined aircrafts. *Table 1* presents the number of aircrafts used in our work. One third part of all three aircraft types used the gates at Terminal 1 and the other two thirds used the gates at Terminal 2. We calculated with a taxi time of 12 minutes for every aircraft.

Table 1. Representative aircraft types and the number of their LTO cycles

Aircraft		LTO cycles during the year 2006
Boeing 737	– medium	57,594
Socata Tampico	– light	3,769
Boeing 767	– heavy	2,112

Emissions are generated by ground support vehicles and auxiliary power units (APUs) while the aircraft is parked at the gate. GSE emissions are obtained from EPA's NONROAD model and are dependent on the age, fuel, horsepower, and load factor applied to the engine. APUs are most often on-board generators that provide electrical power to the aircraft while its engines are shut down. Like GSE, APU emissions generated per LTO cycle are the product of the emission factor and the operating time, and multiplied by the number of applicable aircraft LTO cycles. In case of B737 and B767 the default APUs were used. In case of the other aircrafts (light aircrafts) APUs were not used. The GSE was also set to the default values of the different aircraft types.

In our work, two parking facilities were used next to the two terminals. The model was run using the number of 300,000 vehicles at Terminal 1 and 350,000 vehicles at Terminal 2, in a year. The average speed of vehicles traveling in the parking facility is one of the parameters necessary to determine the emission factors for the movement of the vehicles using MOBILE5a, MOBILE5b, or MOBILE6.2 models. The default fleet mix (types, fuels and ages of vehicles), the speed (10 mph) in the parking facility and the distance (250 m) traveled in lot were set to the default values. The latter is an estimate for the average distance a vehicle travels between entry and exit.

In order to take into account the motor vehicle activity on roadways at and near the airport, it is necessary to use as many traffic count results as possible. The default fleet mix and the speed (56 km h^{-1}) of the vehicles were set to the default values. *Table 2* shows the traffic count data used in our study. Traffic count and the calculations for the whole year was made for 2006.

Table 2. Number of vehicles using the roads in a year near to the airport. Based on traffic count data of 2006

Road	Number of vehicles/year
Preparatory phase of the Motorway 4 (Gyömrői street)	12,469,212
Bypass of the Motorway 4 near Vecsés	6,258,924
Road to Terminal 2	5,763,492
Road between Terminal 1 and Terminal 2	1,200,000

The general methodology for calculating emissions from stationary sources considers the amount of fuel or substance consumed. In the modeling we used the three main stationary sources at the airport. Each of these sources have a stack height of 40 meters and a stack inside diameter of 1.9 meters. *Fig. 2* shows the aerial map of Budapest Ferihegy Airport. The stationary sources, terminals, major roads, monitoring sites, and main ways inside the airport can be seen on the map.

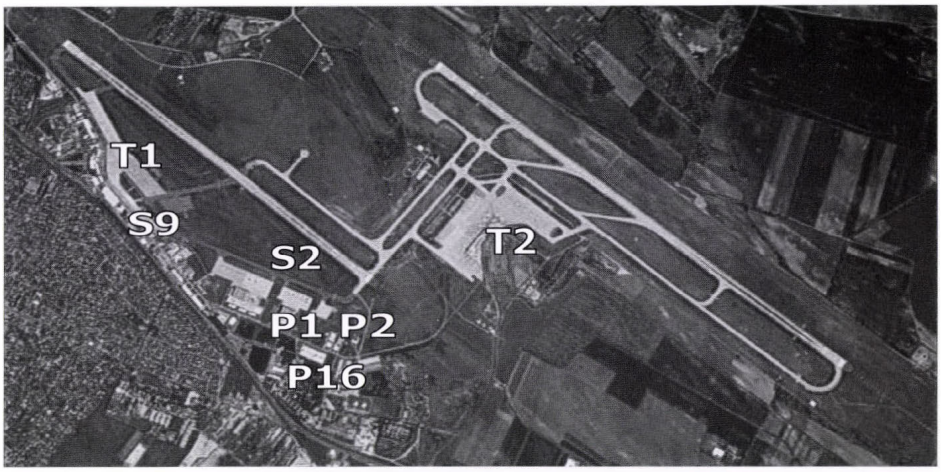

Fig. 2. Aerial map of Budapest Ferihegy Airport. P1, P2, P16: stationary sources; T1, T2: terminals; S2, S9: monitoring sites.

3. Results

Locations at which concentrations are estimated are known as receptors. EDMS allows to consider the placement of receptors in Cartesian or polar coordinate system with the ability to also specify the height of the receptors. In the modeling domain, a Cartesian receptor network was used with different resolutions. Near the main emission sources we used a receptor network with higher resolution (100 m), elsewhere a receptor network with lower resolution (500 m).

Two test runs were made with the EDMS modeling system. The urban ambient NO_x and CO concentrations were not used in the calculations. The EDMS system makes calculation for a whole year cycle using the consecutive modeled meteorological analysis fields and the calculated hourly emission data. The calculated hourly concentration values of the pollutants are then averaged over the year. In the first run we calculated the yearly average NO_x concentration in the receptor points at a height of 1.8 m, based on the meteorological and emission data of the year 2006, in the second run the yearly average CO concentration was calculated in the same way. *Figs. 3* and *4* show the calculated concentrations for NO_x and CO, respectively. In the figures, black solid lines indicate the runways, black dashed lines are taxiways, white solid lines are the main routes next to the airport, and white poligons indicate the two terminals. The numbers at the two axes present the distance in meters from the center (the 0-point) of the figure. The whole area is about 9×8 km^2.

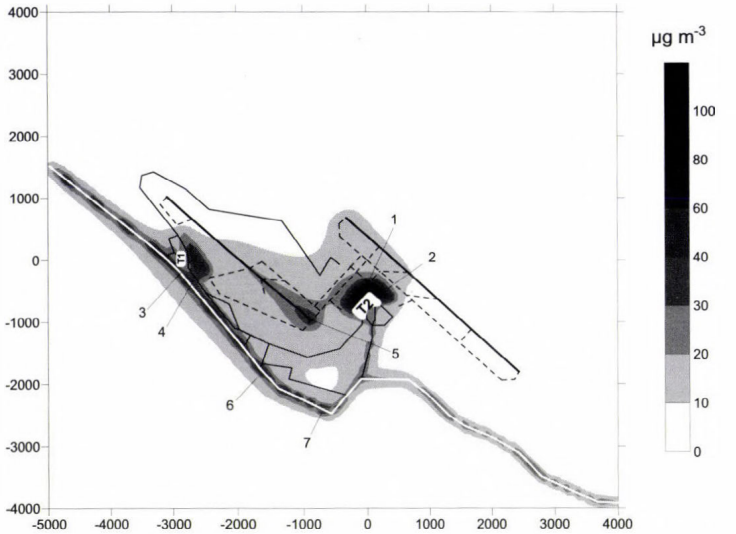

Fig. 3. Yearly average NO_x concentration distribution at Ferihegy Airport, calculated for 2006. Units at the axes are meters.

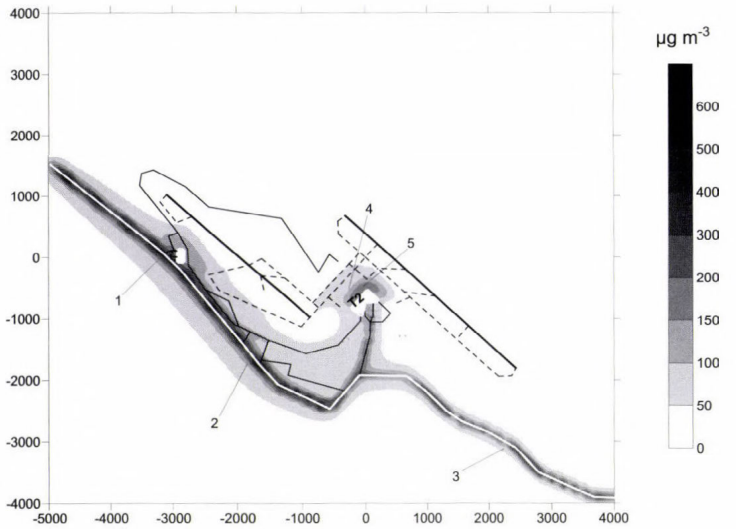

Fig. 4. Yearly average CO concentration distribution at Ferihegy Airport, calculated for 2006. Units at the axes are meters.

Meteorological and emission input data files were constructed on the basis of data, which were observed and calculated for the year of 2006. The pre-processor part of the model makes emission calculations of the different sources

using the input data. After that the dispersion calculations are made. The aim of our modeling work was to determine the concentration distribution of different pollutants near the airport. The main emitted pollutants near the airport are NO_x, CO, PM_{10}, and $PM_{2.5}$. A weakness of the model is that PM emission data is not available for all aircraft engines, thus, we focused on the NO_x and CO concentrations near the airport.

The model calculated the yearly average concentrations at the receptor points. The resolution of the receptor network, used in the model, was not uniform. At the places, where greater emissions occurred, a 100 m receptor network resolution was used. At places, where the emissions are negligible (especially near the edges of the modeling domain), a 500 m receptor network resolution was used. The centre point of the modeling domain is the same as the 0-point of the airport. The geographical coordinates of this point are the following: 47°26'N, 19°15'E. The place of a receptor point is represented with two coordinates. The first coordinate (x-coordinate) shows the distance of the receptor point from the 0-point in east-west direction. In case of positive x-coordinate the receptor point lies east of the 0-point, in case of negative x-coordinate it lies west of the 0-point. The second coordinate (y-coordinate) shows the distance of the receptor point from the 0-point in north-south direction. In case of positive y-coordinate the receptor point lies north of the 0-point, in case of negative y-coordinate it lies south of the 0-point.

Fig. 3 shows the yearly average of the NO_x concentration distribution near the surface of the modeling domain. *Table* 3 presents the receptor points, for which the highest concentrations were found by the model calculations. The place with maximum NO_x concentration can be found at Terminal 2, near the gates (receptor points 1 and 2), with a value of about 100 $\mu g/m^3$. The second highest NO_x concentration values (about 80 $\mu g\ m^{-3}$) can be found near Terminal 1 (points 3 and 4). Because the aircraft traffic is about 25% of the whole traffic at Terminal 1, the concentration values at Terminal 1 are not so high as near Terminal 2. Another maximum place in the NO_x concentration distribution can be found near the starting point of the main runway (receptor point 5). This phenomenon is not strange because the average wind direction near the airport is northwest, so the aircrafts mostly begin the take off cycle from this point (at a specific wind speed value the aircrafts should take off and landing in the direction from where the wind blows). The NO_x emission of the aircraft engines is highest during take off phase, so it is not surprising that the mentioned local maximum place can be found near the most used starting point of the runways. The third place, where the NO_x pollution is significant (about 75 $\mu g\ m^{-3}$) can be found near the motorway No. 4, which runs near the airport (points 6 and 7). This fact is not surprising as the main source of the NO_x pollution is the road traffic. Our calculations show, that in the area of the airport, NO_x emissions of the aircrafts and the vehicles running in the airport and the neighboring motorways give equivalent contributions to the concentration in the ambient air.

Table 3. Locations of the highest yearly average NO_x concentration values

Receptor point	Location	Concentration (μg m^{-3})
1	Terminal 2	102.36
2	Terminal 2	100.93
3	Terminal 1	81.49
4	Terminal 1	81.27
5	Strating point of the runway	92.55
6	Motorway	78.67
7	Motorway	75.79

Fig. 4 shows the yearly average CO concentration distribution near the surface of the modeling domain. *Table 4* presents the receptor points, for which the highest concentrations were found by the model calculations. The first 20 maximum CO concentration values can be found near the motorway No. 4 (receptor points 1, 2, and 3). Concentration values of this 20 receptor points are between 500 and 700 μg m^{-3}. The CO pollution is also significant next to the gates at Terminal 2 (points 4 and 5). The concentration values are here about 200 μg m^{-3}. According to the model calculations, the contribution of the aircrafts to the local ambient CO concentration level is significantly less than the contribution of the ground vehicle traffic.

Table 4. Locations of the highest yearly average CO concentration values

Receptor point	Location	Concentration (μg m^{-3})
1	Motorway	725.48
2	Motorway	711.48
3	Motorway	508.05
4	Terminal 2	211.48
5	Terminal 2	197.25

We can see that in both cases the maximum concentrations are near the gates of Terminal 1 and 2. The maximum yearly NO_x concentrations are about 100 μg m^{-3}, the maximum yearly CO concentrations are about 700 μg m^{-3}. For the maximum concentrations near the gates the GSE and the APUs are responsible. From the emission inventory table of the model it can be seen that GSE and APUs produce the highest CO emissions in the modeling domain. Although the total NO_x emission of the aircrafts and roadways is higher than the NO_x emission of GSE and APUs, aircrafts and vehicles emit the pollutants in a much bigger area. In *Fig. 3* it is visible that in case of NO_x, the vehicles (motorway No. 4) and the moving aircrafts (especially near the starting points, because of the higher NO_x emission in take-off mode) have significant influence in the concentration distribution.

4. Comparison with measurements

In 2006, three measurement campaigns were held to determine the air pollution situation in the area of Budapest Ferihegy Airport. During the measurement campaigns, concentration of numerous air pollutants were detected including common pollutants as nitrogen oxides, carbon-monoxide, and particulate matter, as well as rarely observed pollutants as tire debris and soot particles, which are characteristic of air traffic. The campaigns were performed by the Hungarian Academy of Sciences KFKI Atomic Energy Research Institute. CO, NO, NO_2, SO_2, O_3 and particle mass concentrations were detected in every 2 minutes using gas monitoring equipments (Environnement SA and Airpointer system) and TEOM PM monitor by Thermo. In this study we use hourly averaged NO_x and CO concentrations, measured simultaneously during the second campaign at two places: (i) station 2 was located near ground level, approximately 50 m southwest of the take-off point of one of the runways, and (ii) station 9 was located near ground level, approximately 50 m southwest of the main taxiway to Terminal 1 (see *Fig. 2*).

As the sources at airports show large temporal and spatial variation, and so far we can use observed data measured during short time campaigns, in this first stage of model development we aimed to get a first survey of our results. For this purpose, diurnal variation of hourly averaged concentration values were compared with the modeled values in the period of May 31–June 2, 2006. Based on the results of the measurement campaigns, air pollutant concentrations are going to be monitored continuously at the airport. Thus, in the near future, we plan to make a real validation using the continuously observed data series.

The meteorological situation on the three days of the examined measuring period was rather varied due to the cold front, which crossed Hungary. The sky was generally broken with few hours of sunshine, and showers formed from time to time. There was strong northwest wind with stormy gusts in many places. The maximum temperature was far below the long-time average, 10–17 °C was measured daytime.

There are many papers dealing with the air pollution situation at the airports (*Henry et al.*, 2002; *Yu et al.*, 2004; *Carslaw et al.*, 2006). As the aim of these studies was mainly to detect and quantify aircraft and other on-airport contributions to the ambient air pollution level, they worked with yearly averages of longer data series. Because of the short measuring period, we tried to take a preliminary picture on the temporary pollution situation using hourly averages. *Fig. 5* shows the results of the model calculations for hourly NO_x concentrations compared with the observed data, at stations 2 and 9, during the examined period. The modeled values are increased compared with the ambient NO_x concentration measured at K-puszta (48°58'N, 19°33'E) background monitoring station. The course and order of the modeled and observed data series are very similar, and in most cases, the peaks can be found at the same

time at both measuring sites. This result shows good promise for that we will be able to determine the time and value of the highest peaks of NO_x concentration at both sites.

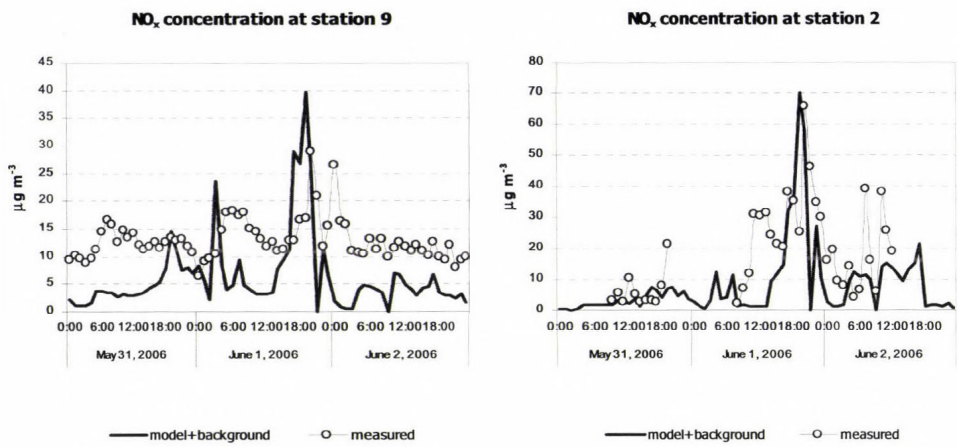

Fig. 5. Comparison of the modeled and measured hourly averages of NO_x concentration at station 2 and 9, during May 31–June 2, 2006.

In case of CO the situation is more complicated. Similarly to NO_x, the modeled CO concentrations were increased compared with the ambient values measured at Hegyhátsál (46°57'N, 16°39'E) background monitoring station. In spite of this, the measured hourly CO concentration values were approximately 100–150 µg m^{-3} higher than the modeled values, and the peaks did not show the same coincidence as in the case of NO_x. The possible reason lies in the buoyant behavior of aircraft plume dilution (*Henry et al.*, 2006), as well as in the fact, which was recognized at other airports: compared with ground vehicle traffic, aircraft do not seem to be a significant source near the airport, at least in terms of producing high concentrations (*Yu et al.*, 2004). CO concentration measured at the area of the airport depends on the wind direction and the CO concentration values in the city, which located in upwind direction from the Budapest Ferihegy Airport. Wind can transport considerable CO pollution from the city, and this effect was not taken into account in the EDMS calculations. It can be assumed, that the missing concentration must be arrived from the areas of Budapest. The wind direction in the examined time period was west, northwest, this fact confirms the previous assumption. This situation must be examined in detail in the near future.

5. *Conclusions*

In this study we presented two model runs using the EDMS airport air quality modeling system. In the first model run the yearly average concentration distribution of NO_x was calculated for the area of the Budapest Ferihegy Airport, based on the calculated hourly concentration values. We saw that the most polluted area was near the gates caused by the emissions of the ground support equipments. Other polluted areas were the starting point of the main runway (effect of the starting aircrafts) and motorway No. 4 (effect of the ground vehicles). In the second run the yearly average concentration distribution of CO was calculated. In this case we could find the most polluted area along motorway No. 4 (effect of the ground traffic). Another polluted area was found near the gates (effect of the ground support equipment). The calculations show, that in the area of the airport, NO_x emissions of the aircrafts and the vehicles running in the airport and the neighboring motorways give equivalent contributions to the concentration in the ambient air, while the contribution of the aircrafts to the local ambient CO concentration level is significantly less than the that of the ground vehicle traffic.

There are three main points which will be further studied in the future. Firstly, we would like to increase the accuracy of our modeling results, mainly in the field of emission input values specific for Budapest Ferihegy Airport. Secondly, as air pollutant concentrations are going to be monitored continuously at the airport, we plan to make a real validation using the measured data series. Finally, the model will be used for calculating the concentration distribution of PM. The main problem is the PM emission data, which is not available for Socata Tampico engines. To solve these problems a lot of measuring work should be completed at and around the airport.

Fortunately, Ferihegy Airport is located in the southeast edge of Budapest, while the prevailing wind direction is northwest. This situation affects the contamination relations advantageously in Budapest. In connection with these work we would like to determine the critical meteorological situations, when high concentration values can be measured next to the terminals.

The sources at airports have large temporal and spatial variation, and concentrations were only measured during short time campaigns. Based on the results of the measurement campaigns, air pollutant concentrations are going to be monitored continuously at the airport. Thus, in the near future, we plan to make a real validation using the continuously observed long time data series.

Acknowledgments—Long-term monitoring of atmospheric carbon monoxide mixing ratio in Hungary is carried out by NOAA ESRL GMD Carbon Cycle and Greenhouse Gases Group (Boulder, Colorado, U.S.A.). The authors thanks them and *Dr. László Haszpra* for making the data available for this study. This paper is supported by the NKFP-JÁP 3/019/2005 National Research Program.

References

Baerentsen, J.H. and *Berkowicy, R.*, 1984: Monte Carlo simulation of plume dispersion in the convective boundary layer. *Atmos. Environ. 18*, 701-712.

Barrett, S. and *Britter, R.*, 2007: A simple approach for rapid operational air quality modelling at airports. *Proceedings of the 11th International Conference on Harmonisation within Atmospheric Dispersion Modelling for Regulatory Purposes.* Cambridge, 2-5 July 2007, 35-361.

Britter, R.E., 2007: The implications of variability of national and regional air quality regulations on the modelling of airport air quality within global aviation/environment models. *Proceedings of the 11th International Conference on Harmonisation within Atmospheric Dispersion Modelling for Regulatory Purposes.* Cambridge, 2-5 July 2007, 335-339.

Carruthers, D., Holroyd, R., Hunt, J.C.R., Weng, W., Robins, A., Apsley, D., Thomson, D., Smith, F., 1994: UK-ADMS: a new approach to modelling dispersion in the earth's atmospheric boundary layer. *J. Wind Eng. Ind. Aerod. 52*, 139-153.

Carruthers, D., McHugh, C., Jackson, M., Johnson, K., 2007: Developments in ADMS-Airport to take account of near field dispersion and applications to the Heathrow Airport. *Proceedings of the 11th International Conference on Harmonisation within Atmospheric Dispersion Modelling for Regulatory Purposes.* Cambridge, 2-5 July 2007, 346-350.

Carslaw, D.C., Beevers, S.D., Ropkins, K., Bell, M.C., 2006: Detecting and quantifying aircraft and other on-airport contributions to ambient nitrogen oxides in the vicinity of a large international airport. *Atmos. Environ. 40*, 5424-5434.

Cimorelli, A.J., Perry, S.G., Venkatram, A., Weil, J.C., Paine, R.J., Wilson, R.B., Lee, R.F., Petersand, W.D., Brode, R.W., Paumier, J.O., 2004: AERMOD: Description of model formulation (EPA-454/R-03-004). US Environmental Protection Agency.

CSSI, Inc., 2004: Emissions and Dispersion Modeling System (EDMS) User's Manual. Prepared for: Federal Aviation Administration Office of Environment and Energy. Washington, DC. FAA-AEE-04-02.

Department for Transport, July 2006: Project for the Sustainable Development of Heathrow – Air Quality Technical Report. www.dft.gov.uk/pgr/aviation

EUROCONTROL Experimental Centre, 2005: Zurich airport 2004: A comparison of modelled and measured air quality. *EEC/SEE/005/017.*

Henry, R.C., Chang, Y.S., Spiegelman, C.H., 2002: Locating nearby sources of air pollution by nonparametric regression of atmospheric concentrations on wind direction. *Atmos. Environ. 36*, 2237-2244.

Janicke, U., Fleuti, E., Fuller, I., 2007: LASPORT – a model system for airport-related source systems based on a Lagrangian particle model. *Proceedings of the 11th International Conference on Harmonisation within Atmospheric Dispersion Modelling for Regulatory Purposes.* Cambridge, 2-5 July 2007, 352-356.

Steib, R. and *Labancz, K.*, 2005: Regulatory modeling in Hungary – the AERMOD model. Part I. Description and application. *Időjárás 109*, 157-172.

Steib, R., 2006: Regulatory modeling in Hungary – the AERMOD model. Part II. Sensitivity of the model and case studies. *Időjárás 110*, 15-33.

U.S. EPA, 2002: User's guide for the AMS/EPA regulatory model – AERMOD. Research Triangle Park, North Carolina.

Weil, I.C., 1988: Dispersion in the convective boundary layer. *Lectures on Air Pollution Modeling* Venkatram, A. and Wyngaard, J.C., American Meteorological Society, 167-227.

Yu, K.N., Cheung, Y.P., Cheung, T., Henry, R.C., 2004: Identifying the impact of large urban airports on local air quality by nonparametric regression. *Atmos. Environ. 38*, 4501-4507.

IDŐJÁRÁS

Quarterly Journal of the Hungarian Meteorological Service
Vol. 112, No. 2, April–June 2008, pp. 113–123

Comparison study in mixing height determination for dispersion models

Tamás Weidinger[1], **Györgyi Baranka**[2] and **Árpád Bordás**[1,3]

[1]*Department of Meteorology, Eötvös Loránd University,*
P.O. Box 32, H-1518 Budapest, Hungary; E-mail: weidi@ludens.elte.hu
[2]*Hungarian Meteorological Service,*
P.O. Box 39, H-1675 Budapest, Hungary; E-mail: baranka.gy@met.hu
[3]*University Centre for Meteorology and Environmental Modelling,*
University of Novi Sad, Trg D. Obradovića 5, 21000 Novi Sad, Serbia;
E-mail: abordas@uns.ns.ac.yu

(Manuscript received in final form June 4, 2008)

Abstract–Hungarian Transmission Standards were updated with the goal of standardising and improving methods for the calculation of meteorological parameters used as inputs in air quality dispersion models. New methods for determining mixing height are recommended by COST 710. For stable and mechanically dominated unstable atmospheric boundary layers, the formula for determining mixing height requires friction velocity, Monin-Obukhov length and Coriolis parameter. For convective boundary layers, a simple prognostic model based on the determination of initial temperature profile, surface momentum and sensible heat fluxes is used. Statistical comparisons among (i) new and (ii) former Hungarian Standards, (iii) AERMOD, (iv) some methods suggested by COST 710 as well as (v) mixing height calculation from radiosonde measurements were performed. Hourly values of mixing height were calculated based on standard meteorological measurements using the different approaches given above for a one-year dataset (1996). Model results for the new Hungarian Standards are in good agreement with radiosonde measurements; the best fit was obtained during periods of a growing convective layer. The growth rate of the mixing layer height is found to be sensitive to the potential temperature gradient above the convective layer.

1. Introduction

In new Hungarian Transmission Standards one chapter deals with the mixing height determination among (i) definitions of meteorological parameters, (ii) description of meteorological measurements at near-surface layer and in the atmospheric boundary layer, (iii) calculation of dynamical parameters of the surface layer, (iv) wind speed, direction and temperature profile and (v) determination of air pollutant dispersion parameters.

Based on hourly standard meteorological measurements, parameterizations (i) of the global radiation and the radiation budget components and (ii) the surface energy budget components (sensible (H) and latent heat (LE) fluxes) were developed using the Penman-Monteith methodology (*De Bruin*, 1983; *Holtslag* and *Van Ulden*, 1983; *Ács*, 1994; *Lagzi et al.*, 2006). Modified Pristley-Taylor parameter was used on the basis of meteorological and agroclimatological information (*Szász* and *Tőkei*, 1997; *Fodor*, 2007). Surface layer parameters, such as friction velocity (u_*), dynamic temperature (T_*), and Monin-Obukhov length (L) were calculated from wind speed (u) and sensible heat flux (H) using Monin-Obukhov similarity theory knowing the roughness length and displacement height (*Weidinger et al.*, 2000; *Ács* and *Kovács*, 2001).

Sources of mixing layer height calculations were (i) formal Hungarian Standards (*Fekete et al.*, 1983; *Szepesi et al.*, 1995, 2005), (ii) the U.S. EPA's AERMOD modeling system (*Cimorelli et al.*, 1998; *Hall et al.*, 2000; *Steib*, 2005; *Steib* and *Labancz*, 2005, *Bozó et al.*, 2006), (iii) results of COST 710 program "Harmonization in the preprocessing of meteorological data for dispersion models" (*Fisher et al.*, 1998) and (iv) the method of *Matyasovszky* and *Weidinger* (1998) using radiosonde measurements.

2. *Mixing height calculation methods to be introduced as New Hungarian Transmission Standards*

2.1. Stable boundary layer

In case of a stable boundary layer three options were applied. If regular upper air measurements were available during the night (at 00:00 UTC), (i) the Richardson number method was used:

$$h = Ri_c \frac{(\Delta u)^2}{\beta \cdot \Delta \Theta_v}, \tag{1}$$

where h is the mixing height, Δu is the difference of wind speed, $\Delta \Theta_v$ is the difference of virtual potential temperature, Ri_c is the critical Richardson number, β is a stability parameter, rate of gravity acceleration and the average temperature of mixing height ($\beta = g/T$). The critical Richardson number was 0.25. (ii) Determination of the top of temperature inversion (h_T) and the level of the local wind maximum (h_u) based on the inflection point of temperature and wind speed and the smaller value ($h = \min(h_T, h_u)$) for the mixing height was chosen.

If upper-air meteorological measurements were not available, then the nocturnal mixing height was parameterised by using (iii) similarity theory (*Zilitinkevich et al.*, 2001; *Zilitinkevich* and *Baklanov*, 2002). Knowing the limitation of the calculation of stable boundary layer height (*Zilitinkevich et al.*,

2007) a traditional form (*Zilitinkevich*, 1972) was used, based on COST 710 (*Fisher et al.*, 1998):

$$h = c \cdot \sqrt{\frac{u_* \cdot L}{f}}, \tag{2}$$

where h is the mixing height (m), u_* is the friction velocity (m s^{-1}), L is the Monin-Obukhov length (m), f is the Coriolis parameter (s^{-1}) and c constant is 0.35.

2.2. Convective boundary layer

In the convective boundary layer a prognostic model derived from simplified formulae of continuity and thermodynamic equations was applied. The increase of mixing layer height caused by thermal turbulence is described by the following differential equation (*Batchvarova* and *Gryning*, 1991):

$$\frac{\partial h}{\partial t} = (1 + 2A)\frac{(-u_* \cdot T_*)}{\gamma_{\Theta_v} \cdot h} + 2B\frac{u_*^3}{\gamma_{\Theta_v} \cdot \beta \cdot h^2}, \tag{3}$$

where h is the mixing layer height, A, B are constants: $A = 0.2$ and $B = 2.5$; $\gamma_{\Theta_v} = \frac{\partial \Theta_v}{\partial z}$ is the virtual potential temperature gradient above the mixing layer, and β is the stability parameter. The first term on the right side of Eq. (3) describes the effect of thermal part of turbulence and the second term describes the mechanical part of the turbulence, which is negligible in most cases.

There is an analytic solution to Eq. (3):

$$\Delta t = t_2 - t_1 = \frac{1}{C^3}\left[\frac{1}{2}(C \cdot h + D)^2 - 2D \cdot (C \cdot h + D) + D^2 \cdot \ln(C \cdot h + D)\right]_{h_1}^{h_2}, \tag{4}$$

where

$$C = \frac{(1 + 2A) \cdot (-u_* \cdot T_*)}{\gamma_{\Theta_v}}, \qquad D = \frac{2B \cdot u_*^3}{\gamma_{\Theta_v} \cdot \beta},$$

h_1 is the height of mixing layer (m) at t_1 starting point of time, h_2 is the height of mixing layer (m) at t_2 given point of time. The mixing height was obtained by iteration using appropriate hourly time step (Δt) as the frequency of the surface synoptic measurements.

Values for two crucial parameters γ_{Θ_v} and $\Delta\Theta$ are needed in this method. γ_{Θ_v} is the virtual potential temperature gradient above the mixing layer determined by radiosonde measurements (γ_{Θ_v}) taking into consideration critical

values of the virtual potential temperature jump at the top of the growing mixed layer ($\Delta\Theta_{vm}$) by Eq. (5) (*Fisher et al.*, 1998):

$$\gamma_{\Theta_v} = \frac{(1+2A)\cdot h - \kappa \cdot B \cdot L}{A \cdot h^2 - \kappa \cdot B \cdot L \cdot h} \cdot \Delta\Theta_{vm} \cdot \tag{5}$$

The growth rate of the mixing layer depends on the value of the virtual potential temperature gradient (γ_{Θ_v}) above the mixing layer. Near surface virtual potential temperature gradient (γ_{Θ_v}) – based on the 00:00 UTC radiosonde measurement – in the stable boundary layer (strong inversion in early morning) has been often underestimated. In this case the virtual potential temperature jump ($\Delta\Theta_{vm}$) has been also underestimated (*Baranka et al.*, 2007).

3. Results

Hourly synoptic meteorological data set as well as 00:00 and 12:00 UTC radiosonde measurements for 1996 from Budapest were used in the development and testing of the new method for calculating the mixing layer height.

3.1. Night time stable stratification

Mixing heights determined from the inflection points of temperature (h_T) and wind (h_u) profiles from the radiosonde measurements ($h = \min(h_T, h_u)$), and from similarity theory (namely Eq. (2)) are very similar during moderate and strong wind speeds ($u(10\text{ m}) > 2\text{ m s}^{-1}$), while in the case of low wind speed the friction velocity ($u*$) is near zero so the estimation of mixing height is uncertain, so a constant value should be used (*Fig. 1*).

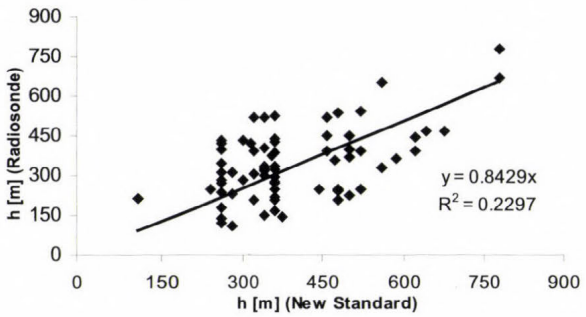

Fig. 1. Mixing height estimation based on radiosonde measurements along with temperature and wind speed, inflection points and similarity theory (New Standard) when the wind speed is higher than 2 m s^{-1} (Budapest, Apr 01, 1996 – Dec 31, 1996, 00:00 UTC).

3.2. *Virtual potential temperature jump above the convective mixing layer*

The behaviour of $\Delta\Theta_{vm}$ and γ_{Θ_v} was investigated using 12:00 UTC radiosonde measurements in the convective cases. The mixing layer height (h) was determined as one of the inflection points of temperature profile.

The critical temperature gradient $\left(\gamma = -\frac{\partial T}{\partial z}\right)$ for (i) the whole mixing layer was > 0.95 °C/100 m and in the upper sublayer it was > 0.8 °C/100 m based on the use of parcel method (*Matyasovszky* and *Weidinger*, 1998).

If the parcel method had not worked (the mechanically driven turbulence, advection, fronts, etc.) the first inflection point of temperature profile was chosen as the mixing height. Of course the mixing height is lower or equal than the cloud base.

In *Fig. 2* the annual course of the virtual potential temperature gradient under (*Fig. 2a*) and above the mixing height (*Fig. 2b*) and the virtual potential temperature jump (*Fig. 2c*) are presented on the basis of radiosonde measurements in Budapest in 1996.

In every month there are few unusable data for determining the mixing layer height by parcel method. Sometimes the virtual potential temperature gradients are very large in the mixing layer (*Fig. 2a*). Incidences of large negative virtual potential temperature gradients and also large positive virtual potential gradients are characteristic of the winter half year. Monthly average virtual potential temperature gradients approach zero in each month. Highest values of monthly average virtual potential temperature gradient above the PBL are formed in summer.

As *Fig. 2b* shows, the virtual potential temperature gradients above the mixing layer are always positive ($\gamma_{\Theta_v} > 0$). Large positive gradients occur in the winter period, with typical values between 0 and 2 °C/100 m. In every season extremely low and high values can be found. However, the monthly averages are larger during the winter than during the summer period. The variability of γ_Θ shows that: the values beneath the mixing height are small, while they are higher above the boundary layer in the free troposphere.

The virtual potential temperature jump ($\Delta\Theta_{vm}$) was also calculated. $\Delta\Theta_{vm}$ is defined as the virtual potential temperature difference in the thin layer (0.1 h) above the top of mixing layer calculated from 12:00 UTC measurements (*Fig. 2c*). The magnitude of $\Delta\Theta_{vm}$ values is between 0.1 °C and 3 °C.

In cases of unstable stratification for each hour the virtual potential temperature jump ($\Delta\Theta_{vm}$) was also calculated by using Eq. (4) during the growth phase of the convective mixing layer. The mixing height was determined by an iterative process. In every time step Eqs. (4) and (5) were solved, and at the same time, the value for γ_{Θ_v} was increased by the actual jump in Θ_{vm}.

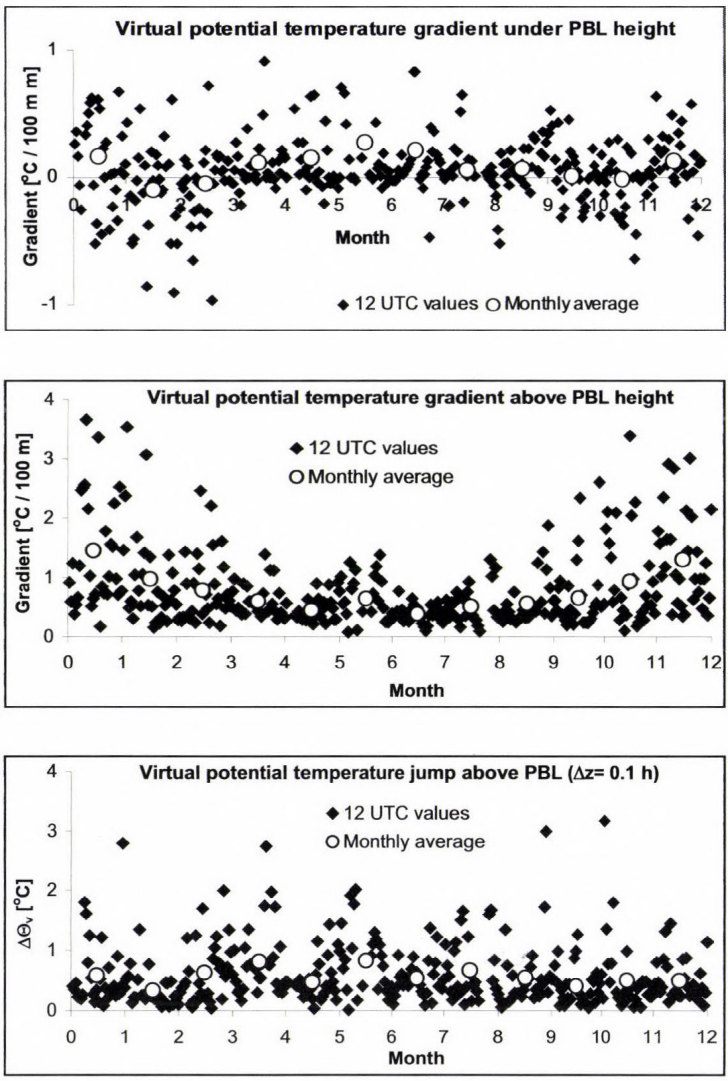

Fig. 2. Time series of the virtual potential temperature gradient under and above mixing height and virtual potential temperature jump above the mixing height in the $\Delta z = 0.1$ h deep layer.

Fig. 3 shows the hourly mixing height values on dependence of $\Delta\Theta_{vm}$ in July (a) and in December (b). High values of $\Delta\Theta_{vm}$ were found around the typical average mixing height for the given season. It means that the increasing rate of mixing height is more intensive in the case of small $\Delta\Theta_{vm}$.

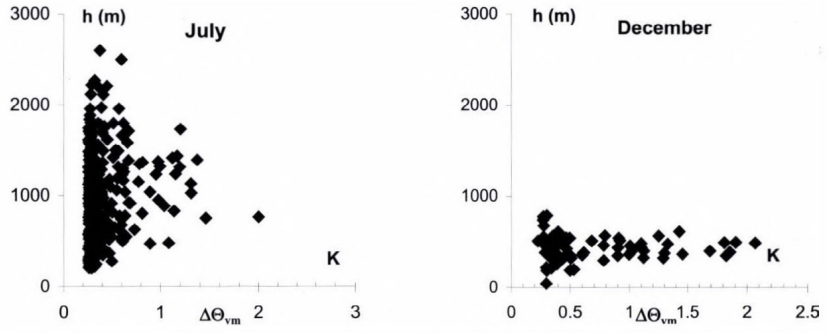

Fig. 3. Hourly values of mixing height (h) against virtual potential temperature jump in July and December of 1996.

The small virtual potential temperature jumps occur at the beginning of the convective growth phase and cases of the well developed mixing height and the larger values of $\Delta\Theta_{vm}$ came from the cases of the moderate mixing heights. The growth rate of the mixing layer $\left(\frac{\partial h}{\partial t}\right)$ is indirectly proportional to the virtual potential temperature jump ($\Delta\Theta_{vm}$).

According to results of numerical experiments, new values of $\Delta\Theta_{vm}$ should be introduced (for lower limit and the upper limit) to check the growth of mixing layer. The new values of potential temperature jump are modified in the following way:

$$\Delta\Theta_{v_m}^{new} = 0.25\ ^{\circ}\mathrm{C}, \quad \text{if} \quad \Delta\Theta_{vm} < 0.25\ ^{\circ}\mathrm{C},$$

$$\Delta\Theta_{v_m}^{new} = 2.25\ ^{\circ}\mathrm{C}, \quad \text{if} \quad \Delta\Theta_{vm} > 2.25\ ^{\circ}\mathrm{C}.$$

The new (corrected) $\gamma_{\Theta_v}^{new}$ is calculated from the Eq. (5).

3.3. Sensitivity analyses of growth of the convective mixing layer height

A sensitivity analysis was carried out to estimate the uncertainty of measurements of meteorological parameters used to determine friction velocity (u_*), virtual potential temperature gradient (γ_{Θ_v}) and dynamical temperature (T_*).

Friction velocity values were modified by ±10% and ±30% during the evaluation the mixing height shown in *Fig. 4*. The example (July 08, 1996) was chosen from the occasional days characterized by quite high insolation. The basic model was developed over a surface covered by grass, and an increase of 30% in u_* over a grass covered surface which is typical over an urban surface

was used and which provides good agreement with radiosonde measurement at Budapest.

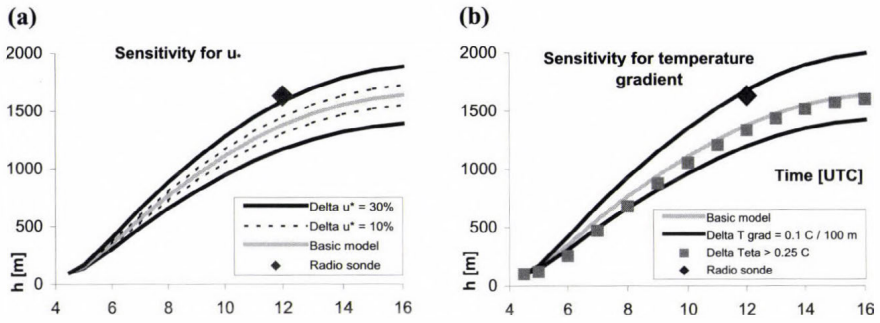

Fig. 4. Sensitivity for u_* (a) and virtual potential temperature gradient (γ_{Θ_v}) above the mixing layer (b) during the growth phase of the convective boundary layer.

The effect of uncertainty in temperature gradient, $\gamma = -\frac{\partial T}{\partial z}$ (or in virtual potential temperature gradient, $\gamma_{\Theta_v} = \frac{\partial \Theta_v}{\partial z}$) above the mixing layer for the calculation of the evaluation of mixing layer height (h) was also examined. The range of uncertainty of temperature gradient (γ) was $\pm$ 0.1 °C/100 m. Mixing layer heights increase more rapidly with larger temperature gradients (smaller virtual potential gradient) than with smaller temperature gradients (larger virtual potential gradient). In this case application of critical values of virtual potential temperature jump has no effect on mixing height. In this case study two mixing height values determined by 12:00 UTC radiosonde data fell within the uncertainty interval of the basic model.

3.4. Comparison study for mixing layer height calculation methods

For validation of mixing height models an intercomparison was carried out using different model formulations. An individual case study of one two-day period from the summer of 1996 is shown in *Fig. 5*. As can be seen from *Fig. 5*, the New Standard method is in good agreement with radiosonde measurements. The methods suggested by COST 710 and the Old Standard method underestimated the mixing layer height measured by radiosonde for about 8 hours during the day on July 15, 1996, otherwise they are also generally in good agreement with the radiosonde measurements. AERMOD generally overpredicted the radiosonde data and showed much poorer agreement with the data than the other three approaches.

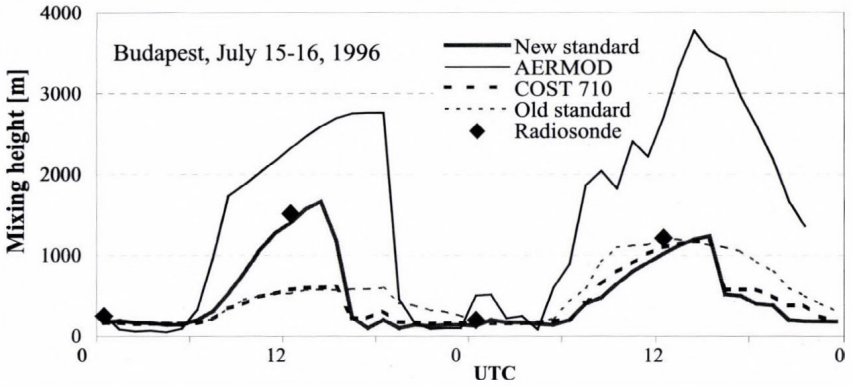

Fig. 5. Evolution and dissolution of mixing layer as computed by different methods.

For each season a statistical study was carried out to establish the characteristics of the four different model approaches comparison with the calculated mixing layer height from the radiosonde data set. *Table 1* gives a summary of results obtained for the summer months at 00:00, 06:00, 12:00, and 18:00 UTC.

The average values and the variances of different models show that there is good agreement between mean values of New Standard and radiosonde measurements at 12:00 UTC. However the New Standard calculated much smaller average values at 00:00 UTC than in the radiosonde data. Mixing height determination in the stable stratification from the inflection points of temperature (h_T) and wind (h_u) profiles from the radiosonde measurements in the case of low wind speed ($u(10\text{ m}) \leq 2\text{ m s}^{-1}$) is uncertain, the mixing heights are often overestimated.

Table 1. Mean values and variances of the mixing height (m) determined by different methodologies at Budapest in summer 1996

	1996 summer season							
	00:00 UTC		**06:00 UTC**		**12:00 UTC**		**18:00 UTC**	
	Mean	**St. dev.**	**Mean**	**St. dev.**	**Mean**	**St. dev.**	**Mean**	**St. dev.**
New standard	153	127	239	155	1349	536	303	597
AERMOD	322	424	451	421	1918	445	453	416
COST 710	140	105	334	660	698	633	284	228
Formal standard	241	73	263	230	1098	494	413	500
Radiosonde	404*	303	-	-	1313	450	-	-

*From top of the temperature inversion (h_T) and from the level of the local wind maximum (h_u) ($h = \min(h_T, h_u)$).

4. Conclusions

In the past years the new meteorological pre-processor for use in transmission models was designed and standardised. The most important part of transmission models is the calculation of the mixing height based on radiosonde and standard meteorological measurements. In the stable case the mixing height was determined using a diagnostic approach, in convective case using prognostic equation. Sensitivity analysis and comparison with other meteorological pre-processors (such as AERMOD, COST 710 recommendations) were done. The new model showed the most acceptable results compared to other mixing height calculation methods.

The advantages of new one-dimensional (1D) mixing layer height calculation model are summarized below:

- Model uses Monin-Obukhov similarity theory to describe the structure of boundary layer.
- Model results provide good agreement with radiosonde data.
- Fundamental input parameters are the potential temperature gradient above the convective layer.
- Growth rate of the mixing height is sensitive to surface fluxes.
- 1D model is easy to use.

Acknowledgements—The work was partly supported by the National Research and Innovation Program (NKFP/088/2004 and 6-00028/2005) and the International Visegrád Found. Special thanks for *Tamás Práger*, *Robert Mészáros,* and *Richárd Kovács* from Department of Meteorology Eötvös Loránd University and *Roland Steib* from Hungarian Meteorological Service for the collaboration in the field of development of meteorological pre-processors for environmental modeling.

References

Ács, F., 1994: A coupled soil–vegetation scheme: description, parameters, validation, and sensitivity studies. *J. Appl. Meteor. 33*, 268–284.

Ács, F. and *Kovács, M.*, 2001: The surface aerodynamic transfer parameterization method SAPA: description and performance analyses. *Időjárás 105*, 165–182.

Baranka, Gy., Weidinger, T., and *Bordás, Á.*, 2007: Analysis of the Hungarian Transmission Standards in mixing heighr determination. *7th Annual Meeting of the European Meteorological Society.* San Lorenzo del El Escorial, Spain, 1-5 October, 2007, EMS2007-A-00395.

Batchvarova, E. and *Gryning, S.E.*, 1991: Applied model for the growth of the daytime mixed layer. *Bound.-Lay. Meteorol. 56*, 261–274.

Bozó, L., Labancz, K., and *Steib, R.*, 2006: Estimation of environmental potential level using dynamical model approach for 2010 in Hungary (in Hungarian). In *Meteorological Scientific Days — Climate Dynamic Researches for Establishment of the Investigation for Estimation of Regional Scale Climate Change* (ed.: *T. Weidinger*). Országos Meteorológiai Szolgálat, Budapest, 207–215.

Cimorelli, A.J., Perry, S.G., Venkatram, A., Weil, J.C., Paine, R.J., Wilson, R.B., Lee, R.F., and *Peters, W.D.*, 1998: AERMOD – Description of Model Formulation. *Version 98315 (AERMOD and*

AERMET) and 98022 (AERMAP)/EPA Document. Posted on EPA Web site. http://www.epa.gov.scram001.

De Bruin, H.A.R., 1983: A model for the Priestley–Taylor parameter *α*. *J. Clim. Appl. Meteorol.* 22, 572–578.

Fekete, K., Popovics, M., and *Szepesi, D.*, 1983: *Guide to Estimate the Transmission of Air Pollutants* (in Hungarian). Országos Meteorológiai Szolgálat Hivatalos Kiadványai LV, Budapest.

Fisher, B., Erbrink, J., Jeannet, P., Joffre, S., Morselli, M., Pechinger, U., Seibert, P., and *Thomson, D.* (eds.), 1998: Harmonisation in the preprocessing of meteorological data for atmospheric dispersion models COST Action 710 Final Report. *EC-DG Science, Research and Development, EUR 18195 EN*, Luxembourg.

Fodor, N., 2007: 4M – Software for Modelling and Analysing Cropping Systems. *J. Univers. Comput. Sci. 12*, No. 9, 1196–1207.

Hall, D.J., Spanton, A.M., Dunkerley, F., Bennett, M., and *Griffiths, R.F.*, 2000: A rewiew of dispersion model inter-comparison studies using ISC, R91, AERMOD and ADMS. *R&D Technical Report P353*, Environment Agency.

Holtslag, A.A.M. and *Van Ulden, A.P.*, 1983: A simple scheme for daytime estimates of the surface fluxes from routine weather data. *J. Clim. Appl. Meteorol. 22*, 517–529.

Lagzi, I., Mészáros, R., Ács, F., Tomlin, A.S., Haszpra, L., and *Turányi, T.*, 2006: Description and evaluation of a coupled Eulerian transport-exchange model. Part I. Model development. *Időjárás 110*, 349–364.

Matyasovszky, I. and *Weidinger, T.*, 1998: Characterizing air pollution potential over Budapest using macrocirculation types. *Időjárás 102*, 219–237.

Steib, R., 2005: Regulatory modeling activity in Hungary. I. In *Advances in Air Pollution Modeling for Environmental Security* (eds.: *I. Faragó, K. Georgiev*, and *Á. Havasi*). Springer, 337–347.

Steib, R. and *Labanc, K.*, 2005: Regulatory modeling in Hungary – the AERMOD model. Part I. Description and application. *Időjárás 109*, 157–172.

Szász, G. and *Tőkei, L.*, 1997: Meteorology for agronomists, horticulturists and foresters (in Hungarian). Mezőgazda Kiadó, Budapest.

Szepesi, D., Fekete, K.E., and *Gyenes, L.*, 1995: Regulatory models for environmental impact in Hungary. *Int. J. Environ. Pollut. 5*, 497–507.

Szepesi, D., Fekete, K., Büki, R., Koncsos, L., and *Kovács, E*, 2005: Development of regulatory transmission modeling in Hungary. *Időjárás 109*, 257–279.

Weidinger, T., Pinto, J., and *Horváth, L.*, 2000: Effects of uncertainties in universal functions, roughness length, and displacement height on the calculation of surface layer fluxes. *Meteorol. Z. 9*, No. 3, 139–154.

Zilitinkevich, S., 1972: On the determination of the height of the Ekman boundary layer. *Bound.-Lay. Meteorol. 3*, 141-145.

Zilitinkevich, S., Baklanov, A., Roost, J., Smedman, A.S., Lykosov, V., and *Calanca, P.*, 2001: Diagnostic and prognostic equations for the dept of the stably stratified Ekman boundary layer. *Danish Meteorological Institute, Scientific Report 01-05*, Copenhagen, Denmark.

Zilitinkevich, S. and *Baklanov, A.*, 2002: Calculation of the height of the stable boundary layer in practical applications. *Bound.-Lay. Meteorol. 105*, 389–409.

Zilitinkevich, S., Esau, I., and *Baklanov, A.*, 2007: Further comments on the equilibrium height of neutral and stable planetary boundary layers. *Q. J. Roy. Meteor. Soc. 133*, 265-271.

IDŐJÁRÁS

Quarterly Journal of the Hungarian Meteorological Service
Vol. 112, No. 2, April–June 2008, pp. 125–139

The influence of global climate change on air and soil temperatures in maize canopy

László Dióssy

Ministry of Environment and Water,
P.O. Box 351, H-1394 Budapest, Hungary; E-mail: diossy@mail.kvvm.hu

(Manuscript received in final form March 7, 2008)

Abstract—On the basis of the climate scenarios downscaled to Hungary from the IPCC Report (*IPCC*, 2007) by *Bartholy et al.* (2007), we performed sensitivity analyses on air temperature in maize canopy. We created the scenario for 2071–2100 by using *Goudriaan*'s (1977) simulation model (Crop Microclimate Simulation Model, CMSM). We selected eight scenarios including the control (1961–1990), one of them examined the changes of the past decade, another one did the impacts of the doubled atmospheric CO_2 concentration. The remaining five scenarios contained different degrees of warming-up beside the doubled atmospheric CO_2 concentration as it follows: scenarios with +3.8, +4.8, +6.0, and two ones with +9.0 °C; the latter two differed only in the quantity of precipitation. Each approach increased the air temperature in maize canopy depending on the degree of warming-up. The changes already occurring in the environmental factors in the past decade increased the air temperature at cob level by 0.6 °C. The presence of plant canopy, however, mitigated the degree of warming-up, likely owing to the shadowing effect of the canopy. We should not ignore the fact that the compensating effect of the canopy depends on the canopy structure determined by the humidity supply. The analysis results made available local level information for the potential users that can provide apparent help in the preparation for the mitigation of adverse impacts of the expected changes.

Key-words: simulation model, air temperature, maize canopy

1. Introduction

Nowadays a lot of Hungarian and foreign studies have been elaborated on the impacts of global warming, as well as one of its cause, the increasing level of the atmospheric CO_2 concentration in the plant physiological processes (*Mihailovic* and *Eitzinger*, 2007; *Mera et al.*, 2006; *Anda* and *Kocsis*, 2007, etc.). The climate scenarios with doubled atmospheric CO_2 concentration attempt to give a picture on the expected changes at different levels (from global to local)

and for periods differing by plant species. The literature interprets doubling of ambient CO_2 concentration as two different values and, therefore, two different time of occurrence. According to the standard interpretation, the doubled ambient CO_2 concentration is 560 ppm, namely the double of the 280 ppm of the period before the industrial revolution. Its realization is expected between 2050 and 2060 as a function of the international CO_2 emission reduction agreements, the innovations in technology and energetics, as well as the world economy's growth. Another interpretation considers 760 ppm, the twofold of the current atmospheric CO_2 level (~380 ppm) as target function; the different scenarios take its expected occurrence time to about 2100 or later (*IPCC*, 2007); as well as in the case of very successful stabilization measures, this level would not be reached in the foreseeable future (see stabilization scenarios of 560 and 680 ppm of the IPCC Report).

The scenarios approximate to the expected temperature with different limit values due to the uncertainty thereof. Global warming is expected to be between 1.1 and 6.4 °C to 2070–2100 in the latest IPCC Report (*IPCC*, 2007). According to *Mika* (2006), a multiplicator of 1.4 should be applied for the Hungarian counterpart; it refers to the higher sensitivity of the Carpathian Basin to the weather changes. In the case of precipitation forecasts the results of the individual GCM runs are very different, on occasion even the signs of the changes differ. Because of the uncertainty exceeding the temperatures in the precipitation forecasts, we laid stress on analyzing the changes in air temperature but not ignoring the changes in precipitation. We applied the scenarios containing the most probable precipitation forecasts for Hungary.

It is not incidental that air temperature is one of the most frequently examined elements of microclimate in researches on plants' environment. Its paramount importance is provided by the fact that ambient air temperature determines the intensity of all physiological processes through influencing biochemical reactions (*Tanner,* 1963; *Graeser et al.,* 1987; *Jacobs et al.,* 1992), based on the temperature optimum curve. Former canopy microclimate observations showed that the air temperatures within plant canopies are different from the temperatures measured on the meteorological station under standard conditions (*Long et al.,* 1964; *Geiger,* 1965; *Jones,* 1983). Observations on maize canopy temperature were synthesized in 1983 by *Warrington* and *Kanemasu* (1983).

With spreading the problem of global warming, it is probable that forecasting the canopy air temperature and the changes thereof will come to the fore again at researches on plants' physiological processes. The aim of our examination was to present the expected changes based on various scenarios in canopy air temperature from the elements of maize microclimate forecast to the area of Keszthely. Topicality of our research was grounded by the appearance of the latest climate scenarios published in IPCC Report (*IPCC*, 2007), and its scenarios downscaled to Hungary's larger regions (*Bartholy et al.,* 2007). The purpose of our analysis was to describe the modifications of these "larger" changes occurring at microclimatic level.

2. *Material and method*

The input data and parameters of the model are derived from the Agrometeorological Research Station at Keszthely (46°44'N; 17°14'E; 114.2 m a. s. l). The input meteorological elements were observed by the local automatic climate station equipped with an Eppley pyranometer, too. Similarly to the meteorological inputs, we used the principle of analogy in the case of the input plant data of the given scenario. As input plant data we looked for data measured in July that was analogous with the weather to be simulated, where the data on maize and soil moisture were the same or almost the same as the values of the year to be simulated. For this we had an about 30-year data series for medium early maturity maize.

The model inputs are site- and plant-specific values (plant height, leaf density in different layers), soil characteristics, and hourly meteorological data (air temperature, global radiation, relative humidity, soil temperatures). The latter data were transformed from the standard measurement levels to the reference levels required by the model. The leaf area and its density were measured in the field on 10 sample plants weekly, using an LI-3000A type leaf area meter.

The soil moisture content in the upper 1 m was also measured in the field with thermo-gravimetric method at 10 cm intervals every 10 days. The actual soil water content was expressed in terms of soil water potential. The physical properties of the Ramann type brown forest soil (heat capacity, heat conductivity, etc.) were determined at the beginning of the investigations. More details on plant and other data samples can be seen in the publication of *Anda* (2006).

The base of the model assumption is the calculation of energy balance in maize canopy after the radiation reflection and transmission processes (*Goudriaan*, 1977; *Goudriaan* and *van Laar*, 1994):

$$0 = R_n - M - Q_H - \lambda E, \tag{1}$$

where R_n is the canopy net radiation (W m^{-2}), M is the metabolic storage (W m^{-2}), Q_H is the sensible heat flux (W m^{-2}), λE is the latent heat flux (W m^{-2}), and λ is the evaporation heat (kJ kg^{-1}).

The sensible heat flux (Q_{Hi}) in the ith layer is:

$$Q_{Hi} = \rho c_p \frac{T_{ci} - T_{ai}}{r_{aHi}}, \tag{2}$$

where T_{ai} is the air temperature in the ith layer (K), T_{ci} is the canopy temperature in the ith layer (K), r_{aHi} is the aerodynamic resistance for sensible heat transfer in the i layer (s m^{-1}), ρ is the air density (kg m^{-3}), and c_p is the specific heat of air (J kg^{-1} K^{-1}).

The latent heat flux (λE_i) in the ith layer can be calculated as follows:

$$\lambda E_i = \rho c_p \{e_s(T_{ci}) - e_i\} / [\gamma(r_{awi} + r_{ci})], \tag{3}$$

where $e_s(T_{ci}) - e_i$ is the difference between the saturation vapor concentration at the plant temperature and the actual vapor concentration ($m^3\ m^{-3}$), r_{awi} is the aerodynamic resistance for water vapor transfer in the ith layer ($s\ m^{-1}$), r_{ci} is the crop resistance in the ith layer ($s\ m^{-1}$), and γ is the psychrometric constant ($0.5\ g\ m^{-3}\ K^{-1}$).

After calculating the sensible and latent heat, the air temperature (T_{ai}) in the ith layer was estimated as:

$$T_{a,i} = T_{a,i-1} + Q_{Hi} R_i / \rho c_p, \tag{4}$$

where R_i is the value characteristic of resistance in the ith layer ($s\ m^{-1}$) when $i=1$ and ($T_{a,i-1}$) is the air temperature for the reference level.

For evaluating the results of the model runs we used paired t-test that was performed by the free version of *STATA 5.0* (1996) program package. The process reduces the two-sample t-test to one-sample test, since there is no possibility of repetition (so of calculation of standard deviation) at the model runs. The test compares the mean value of the sample to an expected mean value. According to the null hypothesis, if the mean value of differences is 0 then the two samples are statistically the same. If the mean value of differences is not 0 then the two samples are significantly different. The significance level was fixed at 5% in the course of the process.

Before applying the Goudriaan model in the present work, the validation of air temperature was carried out locally by *Anda et al.* (2001). The observed air temperature used in the validation of the model was collected in a maize field. To validate the model, the root mean square deviation (*RMSD*) of a number of pairs (n) of simulated (S) and observed (O) elements was applied:

$$RMSD = \left\{ \left[\Sigma (O - S)^2 \right] / n \right\}^{0.5}. \tag{5}$$

The RMSD is one of the best overall measures of model performance (*Willmott*, 1982). More details can be seen in the publication of *Anda* (2006).

2.1. The applied scenarios

The meteorological basis (the control or *first scenario*) of the further scenarios was provided by the mean values of years 1961–1990 measured at Keszthely (*Table 1*), similarly to the reference period of the *IPCC* (2007) scenarios. At the

control run we used the CO_2 concentration measurements performed at Keszthely Agrometeorological Station in the 1980s, as well as the background atmospheric concentration values (1961–1990) from K-puszta and Hegyhátsál (*Dunkel*, 1985; *Haszpra*, 2007) in order to determine the input CO_2 concentration. Finally, we determined the CO_2 concentration of the basic run as 340 ppm. For comparison, *Haszpra* (2007) fixed the Hungarian value for 1981 as 343 ppm.

Table 1. Markings and abbreviations of scenarios used in our investigation. (All meteorological changes refer to the local conditions in July at Keszthely, Hungary.)

Applied scenario	Scenario number	Scenario marking in the figures	Scenario marking in the table of statistical results
Average July data, 1961–1990	1	1961–1990	A
Average data, 1997–2006	2	1997–2006	B
Doubled CO_2 concentration (1961–1990)	3	1961–1990 $2 \times CO_2$	C
Hungarian downscaled values of the B2 SRES scenario*. Precipitation depression: 15% (*Bartholy et al.*, 1997)	4	1961–1990 +3.8 °C	D
Hungarian downscaled values of the A2 SRES scenario*. Precipitation depression: 25% (*Bartholy et al.*, 1997)	5	1961–1990 +4.8 °C	E
6 °C air temperature rise, 25% decrease in precipitation*	6	1961–1990 +6.0 °C	F
9 °C air temperature rise, 10% decrease in precipitation*	7	1961–1990 +9 °C/1	G
9 °C air temperature rise, 30% decrease in precipitation*	8	1961–1990 +9 °C/2	H

*Scenario with doubled CO_2 concentration

The *second scenario* is to represent the changes in the recent past on the basis of the data of the decade between 1997 and 2006. According to the last climate normal, at Keszthely in summer the air temperature is significantly higher by 0.6 °C than the monthly average of all July months in the 1901–2000 data series (*Kocsis* and *Anda*, 2006a). Though it cannot be statistically justified, the accumulated amount of precipitation of July has decreased by about 10–15% at Keszthely (*Kocsis* and *Anda*, 2005, 2006b). We estimated the background CO_2 concentration to be 380 ppm.

The *third scenario* is to represent the impacts of the rising ambient CO_2 concentration in quantitative terms. Therefore, we doubled only the CO_2 gas concentration out of the input data of basic run (760 ppm), and the meteorological inputs remained the same. With this we localized the date of the expected change to 2070–2100.

In the further scenarios – besides doubling the current CO_2 level (760 ppm) –, we gradually increased the air temperature values compared to the basic run (1961–1990), and together with this we also modified the precipitation amount. The *fourth scenario*, based on the B2 scenario (*Nakićenović* and *Swart*, 2000), also applied by the recent IPCC Report (*IPCC*, 2007) contained the summer values pertaining to the Keszthely meteorological elements elaborated and mapped for Hungary by *Bartholy et al.* (2007), and made a forecast to the period of 2070–2100. In this scenario the summer average air temperature at Keszthely will be risen by 3.8 °C, together with an about 15% decrease in precipitation. The *fifth scenario* used the summer data according to the A2 SRES scenario (*Nakićenović* and *Swart*, 2000), downscaled to Hungary by the above-mentioned method, which calculated stronger warming than the former one (+4.8 °C). There is a 25% decrease in the precipitation amount associated to this temperature rise. We note here, that standard deviation is rather high in both scenarios (±15%); this implies strong uncertainty.

In the *sixth scenario* we increased the average air temperature by 6.0 °C, together with 25% decrease in precipitation. This 6 °C rise is close to the upper limit (6.4 °C) of changes related to the annual global mean temperature in the IPCC Fourth Assessment Report (*IPCC*, 2007). However, summer temperature changes can be stronger in Hungary than the global mean warming (*Mika*, 2006). Keeping this in view, in the last two scenarios we presumed a further increase in the warming-up, by involving the product of the 1.4 times higher temperature rise (6.4 °C) pertaining to Hungary (9 °C). Since we knew the uncertainty of precipitation forecasts, we associated two types of precipitation supply to these +9 °C projections: the *seventh scenario* assumed almost no change in precipitation (–10%), while the *eighth scenario* calculated more significant drying (30% precipitation decrease). The comparison of these latter two scenarios later provided opportunity to quantify the impacts of the different precipitation supplies on the plants. Markings of the individual scenarios are summarized in *Table 1*.

3. Results and discussion

The observations on air temperature in maize canopy are of importance since C_4 plants are less sensitive to the changes in the environmental elements than C_3 plants, their radiation and temperature reactions given to global warming showed as being significant (*Mera et al.*, 2006).

In all the scenarios the increased surrounding temperature has increased the canopy air temperature at the cob level, where plant physiological processes are most intensive. The degrees of the warming-up within canopy at cob level were not significantly different by the sun angle (*Fig. 1*), though at the warmer scenarios (from the *fourth scenario*) the peak of maximum temperatures tendentiously occur one hour later, at 3 p.m. instead of 2 p.m.

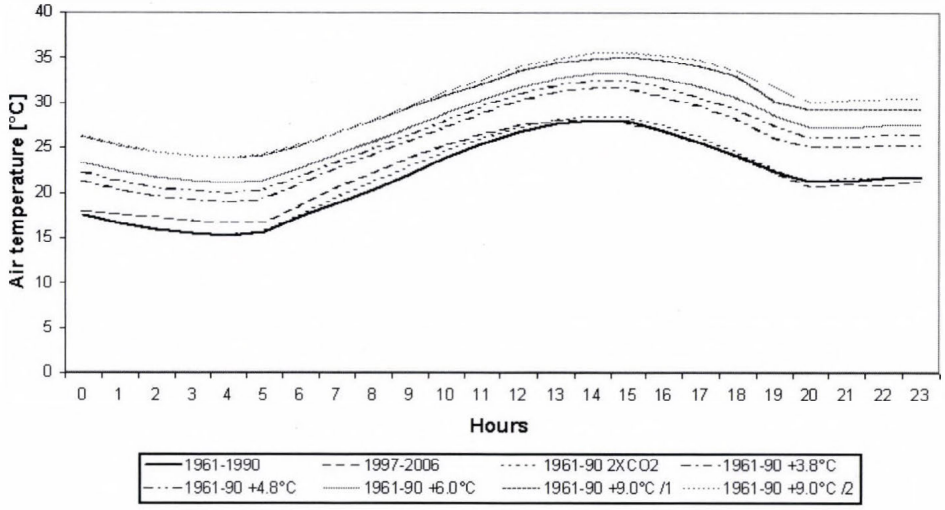

Fig. 1. Air temperature course within maize canopy at cob level, on an average day in July, Keszthely. The height of the simulation is 1 m above the soil surface.

Keszthely was affected by the global warming in the past decade as regards the canopy inside air temperature. During the comparison the temperature rise at the cob level followed the rise of the ambient air temperature compared to the 1961–1990 climate normal serving as basis in many researches; the increase was 0.6 °C compared to the average of the 1961–1990 years on an average day in July. The change is significant at high level (*Table 2*).

Doubling the atmospheric CO_2 concentration [the single input parameter out of the inputs of the basic run (1961–1990)] has significantly increased (by 0.3 °C) the canopy air temperature at the cob level; this indicated the stimulating effect on the pores by the higher CO_2 concentration on the movements of stomata. Stimulation of the closure of stomata controls the transpiration (and also the CO_2 gain), and this energy may emerge as surplus at other energy consuming processes, for example one of the components of sensible heat. According to *Fulco* and *Asseng* (2006), a 50% rise in CO_2 level would compensate the impacts of a 2 °C warming-up and 15% decrease in precipitation amount as the result of the effects on stomata. The authors also noted that the impact is not linear, so, for example, it is not suitable to compensate the impacts of a 4 °C warming-up deriving from a 100% rise in CO_2 level.

The comparison among the first and third scenarios and the results of runs of IPCC origin shows, that the connection of warming-up and doubling the CO_2 concentration together interacted in a way inducing a "milder" change in canopy air temperature. This corresponds with the former experience of *Prasad et al.* (2006).

Table 2. Basic data of statistical analyses relating to the differences of the daily average air temperatures at the cob level. Bold letters highlight *p* values of the t-test, which represent significant difference at level of at least 5%. At the compared scenarios bold and italic letters are used for the basic run

Scenario pairs	Average temperature [°C]	Calculated *p* value of t-test	Standard error
A = basic	21.7		
B	22.2	**0.0025**	0.169
C	21.9	**0.0001**	0.062
D	25.3	**0.0000**	0.038
E	26.3	**0.0000**	0.060
F	27.3	**0.0000**	0.096
G	29.5	**0.0000**	0.147
H	29.9	**0.0000**	0.149
G = basic	29.5		
H	29.9	**0.0000**	0.086
D = basic	25.3		
E	26.3	**0.0000**	0.040
F = basic	27.3		
G	29.5	**0.0000**	0.092
H	29.9	**0.0000**	0.057

At scenarios simulating the change downscaled to Hungary (A2 and B2 scenarios), the degree of warming-up within the canopy fell from the growth level of surrounding air temperature used regarding the warming-up; the conclusion is that the presence of the canopy slightly compensates the warming-up. The compensation degrees were the same at both scenarios (0.2 °C). The degrees of change of the canopy air temperature given to the outer environmental force were of similar tendencies at both scenarios of IPCC origin, but regarding the magnitude, they followed the temperature changes simulated in the warming-up being significantly different from each other. This means that the absolute values of warming-up were different in the two scenarios, only the degrees of change compared to the control values were the same. Warming-up of the canopy of A2 scenario significantly exceeded the value of B2 scenario.

In the case of the last two increased global warming scenarios, the compensating effect of maize canopy on the air temperature at cob level endured, however, it strongly depended on the soil moisture level. Assuming less decrease in precipitation (–10%), the presence of the canopy could mitigate the 9 °C ambient warming-up by 1.2 °C. This is likely owing to the stronger shadowing effect of larger green surface, which could be developed as a result of the better water supply. If we connect the warming-up of the above-mentioned degree with a more significant decrease in precipitation, and we analyze it assuming the presence of a lesser shadowing green surface together

with this (plant-analogy), the compensating effect is immediately halved, to about 0.7 °C.

Warming-up within the canopy results in a statistically justifiable change in all scenarios (see *Table 2*).

The temperature simulation of the model (air temperature above soil, soil temperature) extends from 50 cm below surface to the height of 3 m above soil surface (*Fig. 2*).

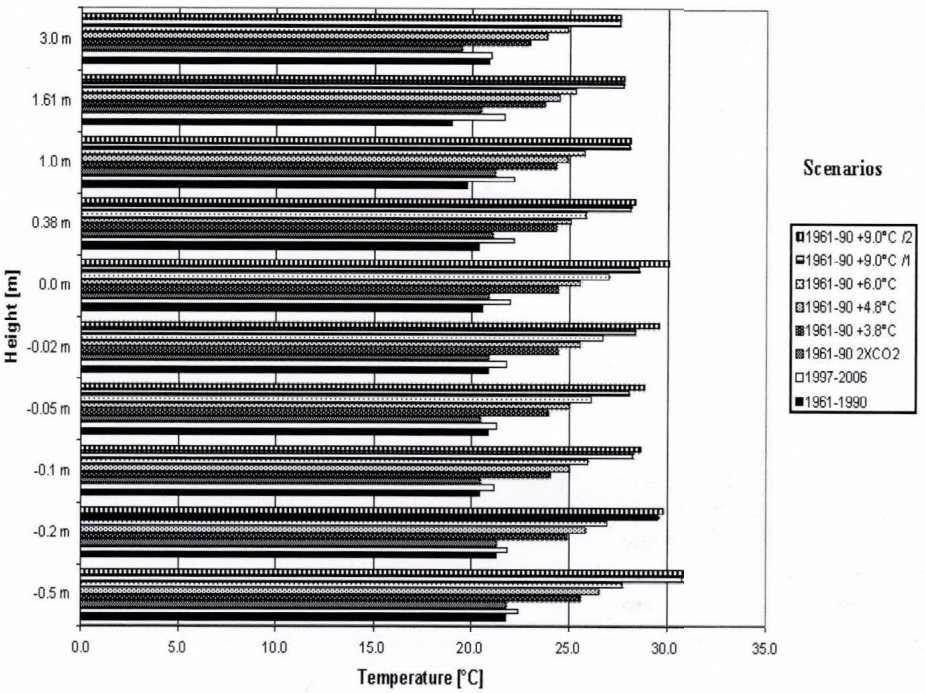

Fig. 2. Estimated air and soil temperature values in case of different climatic scenarios and different levels, at low solar angles (at 9 a.m.).

The levels representing soil temperatures with negative sign (2, 5, 10, 20, and 50 cm) correspond with the locations of soil temperature measurements applied at standard meteorological observations. At 9 a.m. the slightly higher soil temperatures of the deeper layers can be seen at each scenario. The temperature of the air layer above the canopy between 1.8–2.0 m (3 m) determined to low solar position – in accordance with former observations – is cooler above each treatment than the value calculated to the canopy level of 1.6 m.

Except for the scenario assuming the doubled CO_2 level with unchanged air temperature, the temperature of the air is a bit warmer in the layer closest to the soil, and further to the upper layers in the canopy it is slightly decreasing.

Exclusively at the doubled CO_2 level in the morning, the air temperature at cob level and above canopy has increased by a couple of tenths °C compared to the layer close to the soil, and has only decreased above 3 m of the canopy. It refers to the fact that at doubling the CO_2 concentration the energy balance has been modified, and a larger part of the energy balance has remained in the canopy and a smaller part has been transferred to the air above the plant stand. Scenarios with increased air temperature and doubled atmospheric CO_2 concentration transferred more energy to the ambient air above the canopy.

We also illustrate the changes of air and soil temperatures through another vertical profile with different grouping, where the individual scenarios form a category on the vertical axis of the figure (*Fig. 3*). In this case we can follow the expected temperatures of the scenarios one by one, from the depth of 50 cm in the soil up to 3 m in the air. The highest point above soil surface exceeds the top point of the canopy by 1–1.2 m. Ordering of the scenarios occurred by the increasing degree of warming-up, it is well reflected by the length of the columns of the graph. As we go up with the scenarios simulating larger and larger warming-up, warmer and warmer plant canopy develops in terms of soil and air in the morning.

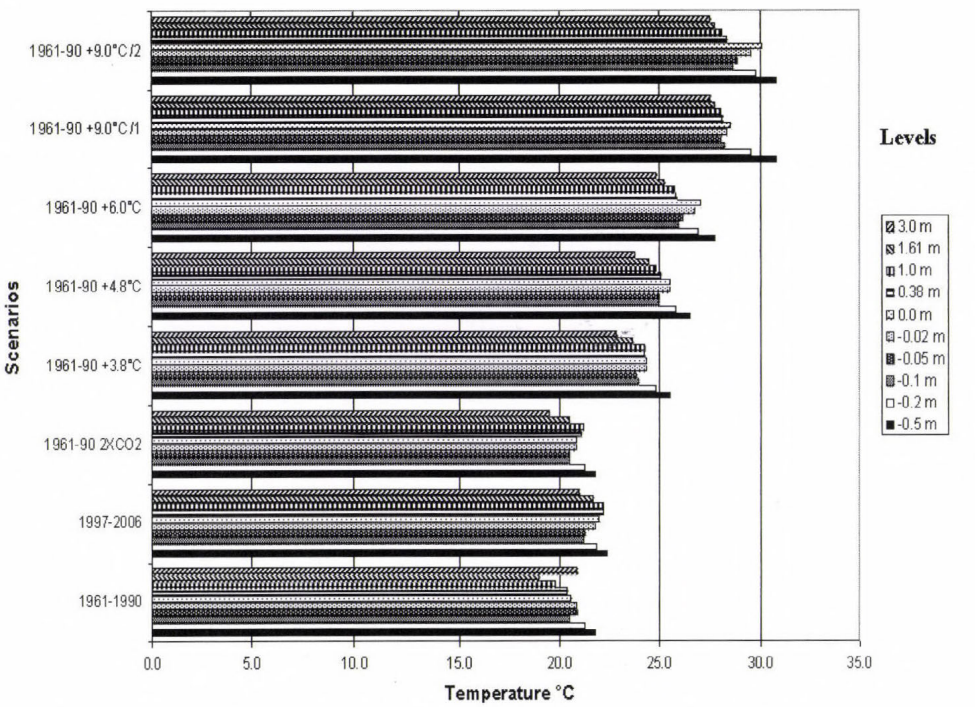

Fig. 3. Estimated air temperature and soil temperature values in case of different climatic scenarios and different levels, at low solar angles (at 9 a.m.).

At high insulation the temperature differences between the different levels are increasing both in the soil and air (*Fig. 4*). As a result of the intensive radiation, the temperature of the soil layers close to the surface are rising quicker than that of the deeper layers. The warmest level is the soil surface. At the warming-up simulation of above 4.8 °C, the soil temperature of the layer of 2 cm reaches or exceeds 30 °C at least. It should be noted that the presented soil temperature is within the canopy, so it is exposed to the shadowing effect of the plants, therefore, it can not be considered as extremely high.

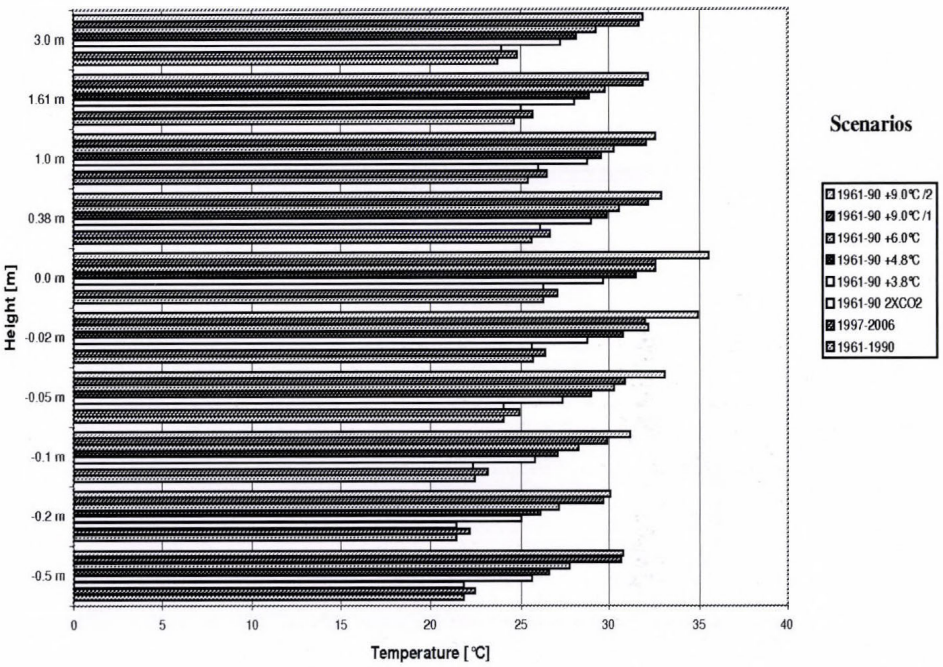

Fig. 4. Expected air and soil temperatures at high solar incoming radiation (at 12 a.m.) at Keszthely. The levels of soil temperature are marked with negative sign. 0.0 m means soil surface.

Similarly to the differences of soil and air temperatures presented at low solar angle by scenarios, the warmer or cooler statuses of canopies of scenarios representing different warming-up levels can also be well seen in the presentation containing high incoming solar radiation (*Fig. 5*). The cooler status of the scenarios with only doubled CO_2 concentration compared to the other scenarios has also remained at the high incoming radiation level.

In the simulations, at noon the frequency of events reaching and exceeding 30 °C has increased. At the run representing the warming-up forecast of 9 °C, the temperature of the entire canopy – both below and above soil surface – exceeds 30 °C, which is far higher than the desired optimal temperature for maize, 23 °C.

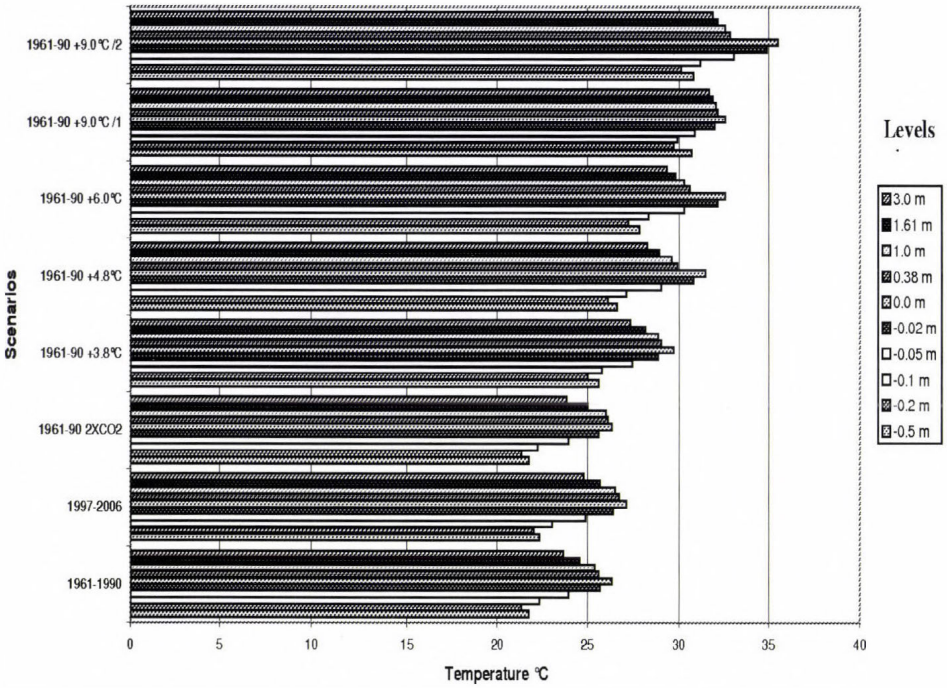

Fig. 5. Estimated air and soil temperature values in case of different climatic scenarios and different levels, at high solar radiation (12 a.m.).

3.1. Development of carbon assimilation

In the Julies of the past decade, both the unit green surface area and the CO_2 assimilation capacity per unit soil surface rose by about 7% in maize (*Table 3*). An increased atmospheric CO_2 concentration itself would enhance the CO_2 assimilation of canopy by about 40%.

In B2 run the entire canopy carbon assimilation above leaf and soil showed an increase compared to the control scenario at both levels, at leaf level the rise was higher, by 24.7%, while the unit value at the soil (canopy level) was lower, by 13.8%. In the case of A2 scenario, the assimilation change was positive only at the leaves, and this value was lower about 10% (14.4%) than the determined value of B2 scenario. The development trend of the average July carbon assimilation per unit soil surface at canopy level was of different direction and degree than it occurred in the case of leaves; the depression of 9.4% compared to the July averages of 1961–1990 emerging at A2 scenario provides a good characterization thereof. In our scenarios simulating a warming-up over 6 °C, the carbon assimilation of both the leaves and the entire canopy has decreased compared to the control run. The depression occurring in the assimilation of leaves has especially emerged at the scenario representing a warming-up of 9 °C,

associated with stronger water deficit. The very strong decrease emerging in carbon assimilation determined to the canopies (soil surface) and exceeding leaves is considerable, which is almost 50% at a scenario simulating a monthly average warming-up of 6 °C; it is 62.5% at runs containing a warming-up of 9 °C, with a decrease in precipitation of 10%; and it is 95.3% in the case of applying a water deficit of 30%.

Table 3. Daily average of carbon assimilation in kg related to unit leaf [m^2] and soil surface area [m^2] during July, at Keszthely. *The values in % represent the differences in photosynthesis of scenarios compared to control run

Scenario/ (kg CO_2 m^{-2})	**1961–1990**	**1997–2006**	**Basic 2×CO_2**	**B2**	**A2**	**+6 °C**	**+9 °C/1**	**+9 °C/2**
CO_2 assimilation per unit leaf area in kg	1.35	1.45	2.02	1.73	1.56	1.32	1.32	1.03
*Change in % to control run	0.0	7.14	39.76	24.68	14.43	–2.25	–2.25	–26.89
CO_2 assimilation per unit soil surface in kg	3.78	4.05	5.66	4.34	3.44	2.38	1.98	1.34
*Change in % to control run	0.0	6.90	39.83	13.79	–9.42	–45.45	–62.50	–95.31

4. Conclusions

The canopy air temperature in each scenario has significantly warmed at high probability level compared to the basic run. In the past decade its degree was 0.6 °C compared to the 1961–1990 period. Warming-up of the canopy changed proportionally to the increase in ambient air temperature. According to the investigations of *Lobell* and *Field* (2007), warming-up of plant stands would expectedly have an adverse impact on plant species belonging to various plant physiological groups, so on C_4 maize.

Comparison of the different runs shows that the change of either the air temperature or the atmospheric CO_2 concentration itself will not result in appropriate outcome, since these factors may strengthen or suppress each other's effects. In accordance with this, the different precipitation supplies of the last two scenarios (7th and 8th) caused significant difference in the canopy air temperatures. We should be cautious because of the significantly different reactions regarding canopy air temperature at both runs containing air temperature increase of 9 °C compared to warming-up of 6 °C.

Our own investigations confirmed the former statement of *Prasad et al.* (2006), that the impact of the increased atmospheric CO_2 gas concentration, which enhances the intensity of photosynthesis cannot be always realized due to

the accompanying warmer plant and air temperature, so it is not expedient to calculate with the emergence of monthly average summer warming-up of above 6 °C at Keszthely; this positive effect is associated to one of the causes of global warming, the higher CO_2 concentration.

These scenarios – opposite to the data on global warming – could even provide insight into the issue of weather and CO_2 concentration changes and plant reactions for the local farmers. Local level information could provide apparent help for the local farmers in the preparation for defending against the adverse effects of the expected changes.

References

Anda, A., 2006: Modeling maize response to climate modification in Hungary. *Commun. Biometry Crop Sci. 1* (2), 90-98.

Anda, A. and *Kocsis, T.*, 2007: Evaluation of the influence of climatic changes on maize energy consumption in Hungary. GSB. *The Eur. J. Plant Sci. and Biotech. 1, 200-205.*

Anda, A., Lőke, Zs., and *Burucs, Z.*, 2001: Microclimate of irrigated and non irrigated maize (in Hungarian). *Növénytermelés 50*, 249-260.

Bartholy, J., Pongrácz, R., and *Gelybó, Gy.*, 2007: Regional climate change in Hungary for 2071-2100. *Applied Ecol. and Environ. Res. 5,* 1-17.

Dunkel, Z., 1985: Vertical profiles of CO_2 in maize canopy (in Hungarian). *Beszámolók az 1982-ben végzett tud. kutatásokról*. Országos Meteorológiai Szolgálat, Budapest, 82-97.

Fulco, L. and *Asseng, S.*, 2006: Climate change impacts on wheat production in a Mediterranean environment in Western Australia. *Agr. Syst. 90,* 159-179.

Geiger, R., 1965: *The Climate Near the Ground*. Harvard Univ. Press, Harvard, Mass.

Graeser, E.A., Verma, S.B., and *Rosenberg, N.J.*, 1987: Within canopy temperature patterns of sorghum at two row spacings. *Agr. Forest Meteorol. 41,* 187-205.

Goudriaan, J., 1977: *Crop Micrometeorology: A Simulation Study*. Simulation Monographs. Pudoc, Wageningen.

Goudriaan, J., and *van Laar, H.H.*, 1994: *Modelling Potential Crop Growth Processes*. Kluwer Academic Publishers, Dordrecht-Boston-London, 238 pp.

Haszpra, L., 2007: 25 years history of CO_2 measurements in Hungary (in Hungarian). *Légkör 52*, No.1, 4-7.

IPCC, 2007: Climate Change 2007: The Physical Science Basis. Contribution of Working Group I to the Fourth Assessment Report of the Intergovernmental Panel on Climate Change [*Solomon, S., D. Qin, M. Manning, Z. Chen, M. Marquis, K.B. Averyt, M. Tignor* and *H.L. Miller* (eds.)]. Cambridge University Press, Cambridge, United Kingdom and New York, NY, USA, 996 pp. Available: http://www.ipcc.ch/pdf/assessment-report/ar4/wg1/ar4-wg1-frontmatter.pdf

Jacobs, A.F.G., van Boxel, J.H., and *Shaw, R.H.*, 1992: Horizontal and vertical distribution of air temperature in a vegetation canopy. *Neth. J. Agr. Sci. 40*, 359-372.

Jones, H.G., 1983: *Plants and Microclimate*. Cambridge University Press. Cambridge-London-New York-New Rochelle-Melbourne-Sydney, 323 pp.

Kocsis, T. and *Anda, A.*, 2005: Tendency in yearly precipitation sums at Keszthely as a result of 130 year observation (in Hungarian). *Légkör 50,* 2, 16-20.

Kocsis, T. and *Anda, A.*, 2006a: The air temperature at Keszthely in 20th century (in Hungarian). *Légkör 51,* 1, 21-24.

Kocsis, T. and *Anda, A.*, 2006b: The precipitation at Keszthely by investigating long time series (in Hungarian). *J. Central Eur. Agric. 7,* 699-708.

Lobell, D.B. and *Field, C.B.*, 2007: Global scale climate–crop yield relationships and the impacts of recent warming. *Environ. Res. Letters 2,* 14-21.

Long, I.F., Monteith, J.L., Penman, H.L., Szeicz, G., 1964: The plant and its environment. *Meteorol. Rundsch. 17*, 97-101.

Mera, R.J., Niyogi, D., Buol, G.S., Wilkerson, G.G., and *Semazzi, F.H.M.*, 2006: Potential individual versus simultaneous climate change effects on soybean (C3) and maize (C4) crops: An agrotechnology model based study. *Global Planet. Change 54*, 163-182.

Mihailovic, D.T. and *Eitzinger, J.,* 2007: Modelling temperatures of crop environment *Ecol. Model. 202,* 465-475.

Mika, J., 2006: Preparation of climatic scenarios by using statistical methods (in Hungarian). *Theses of DSc Degree,* Hungarian Academie of Sciences, Budapest, 143 pp.

Nakićenović, N. and *Swart, R.* (eds.), 2000: *Special Report on Emissions Scenarios. A Special Report of Working Group III of the Intergovernmental Panel on Climate Change.* Cambridge University Press, Cambridge, United Kingdom and New York, NY, USA, 599 pp.

Prasad, P.V.V., Boote, K.J., Allen, L.H. Jr., 2006: Adverse high temperature effects on pollen viability, seed-set, seed yield and harvest index of grain-sorghum are more severe at elevated carbon dioxide due to higher tissue temperatures. *Agr. Forest Meteorol. 139*, 237-251.

STATA 5.0, 1996: Stata Corporation LP Texas, USA. Available online: www.stata.com

Tanner, C.B., 1963: Plant temperatures. *Agron. J. 55*, 210-214.

Warrington, I.J. and *Kanemasu, E.T.*, 1983: Corn growth response to temperature and photoperiod. *Agron. J. 75*, 749-75.

Willmott, C.J., 1982: Some comments on the evaluation of model performance. *B. Am. Meteorol. Soc.*, 1309-1313.

GUIDE FOR AUTHORS OF *IDŐJÁRÁS*

The purpose of the journal is to publish papers in any field of meteorology and atmosphere related scientific areas. These may be

- research papers on new results of scientific investigations,
- critical review articles summarizing the current state of art of a certain topic,
- short contributions dealing with a particular question.

Some issues contain "News" and "Book review", therefore, such contributions are also welcome. The papers must be in American English and should be checked by a native speaker if necessary.

Authors are requested to send their manuscripts to

Editor-in Chief of IDŐJÁRÁS

P.O. Box 39, H-1675 Budapest, Hungary

in three identical printed copies including all illustrations. Papers will then be reviewed normally by two independent referees, who remain unidentified for the author(s). The Editor-in-Chief will inform the author(s) whether or not the paper is acceptable for publication, and what modifications, if any, are necessary.

Please, follow the order given below when typing manuscripts.

Title part: should consist of the title, the name(s) of the author(s), their affiliation(s) including full postal and e-mail address(es). In case of more than one author, the corresponding author must be identified.

Abstract: should contain the purpose, the applied data and methods as well as the basic conclusion(s) of the paper.

Key-words: must be included (from 5 to 10) to help to classify the topic.

Text: has to be typed in single spacing with wide margins on one side of an A4 size white paper. Use of S.I. units are expected, and the use of negative exponent is preferred to fractional sign. Mathematical formulae are expected to be as simple as possible and numbered in parentheses at the right margin.

All publications cited in the text should be presented in a *list of references*, arranged in alphabetical order. For an article: name(s) of author(s) in Italics, year, title of article, name of journal, volume, number (the latter two in Italics) and pages. E.g., *Nathan, K.K.*, 1986: A note on the relationship between photo-synthetically active radiation and cloud amount. *Időjárás 90,* 10-13. For a book: name(s) of author(s), year, title of the book (all in Italics except the year), publisher and place of publication. E.g., *Junge, C.E.*, 1963: *Air Chemistry and Radioactivity*. Academic Press, New York and London. Reference in the text should contain the name(s) of the author(s) in Italics and year of publication. E.g., in the case of one author: *Miller* (1989); in the case of two authors: *Gamov* and *Cleveland* (1973); and if there are more than two authors: *Smith et al.* (1990). If the name of the author cannot be fitted into the text: *(Miller,* 1989); etc. When referring papers published in the same year by the same author, letters a, b, c, etc. should follow the year of publication.

Tables should be marked by Arabic numbers and printed in separate sheets with their numbers and legends given below them. Avoid too lengthy or complicated tables, or tables duplicating results given in other form in the manuscript (e.g., graphs)

Figures should also be marked with Arabic numbers and printed in black and white in camera-ready form in separate sheets with their numbers and captions given below them. TIF, GIF or BMP formats should be used for electronic artwork submission.

The text should be submitted both in manuscript and in electronic form, the latter in e-mail or CD. MS Word format is preferred.

Reprints: authors receive 30 reprints free of charge. Additional reprints may be ordered at the authors' expense when sending back the proofs to the Editorial Office.

More information for authors is available: antal.e@met.hu

Published by the Hungarian Meteorological Service

Budapest, Hungary

INDEX: 26 361

HU ISSN 0324-6329